A

	non-metastatic		metastatic
	D2.0R	D2.1	D2A1
in vitro, monolayer (2D)			
proliferation (% Ki67-positive)	59	65	66
apoptosis (% TUNEL-positive)	3	2	1
in vitro, Matrigel on-top (MoT; 3D)			
proliferation (% Ki67-positive)	17	17	71
apoptosis (% TUNEL-positive)	6	6	6
in vivo, in the lungs after tail vein injection			
extravasation (relative # of extravasated cells)	88	105	100
proliferation (% BrdU-positive after 6h pulse)	4	6	37
apoptosis (% cleaved-caspase-3-positive)	4	2	2

E

(orthotopic implantation)	tumor incidence
D2.0R	24/24
D2.1	20/22
D2A1	22/22

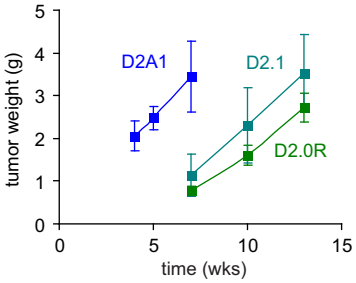

B

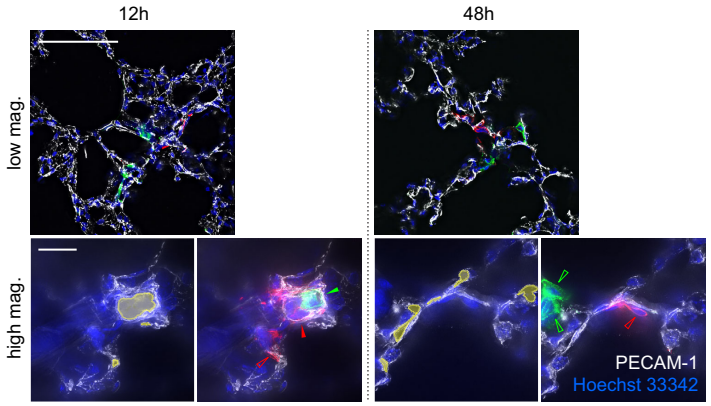

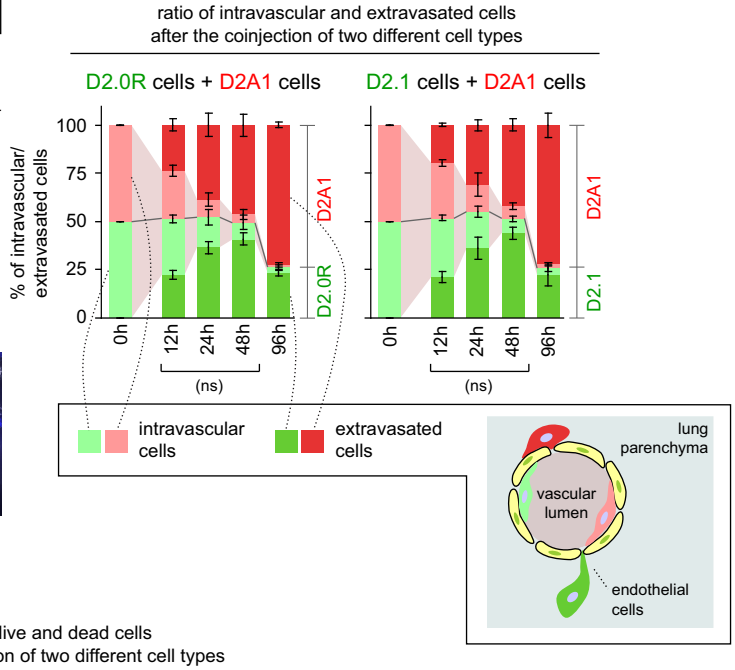

C

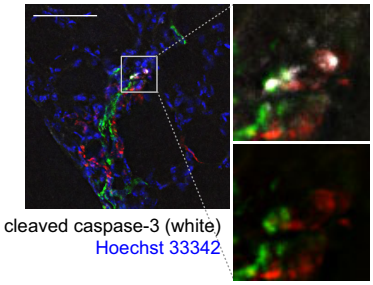

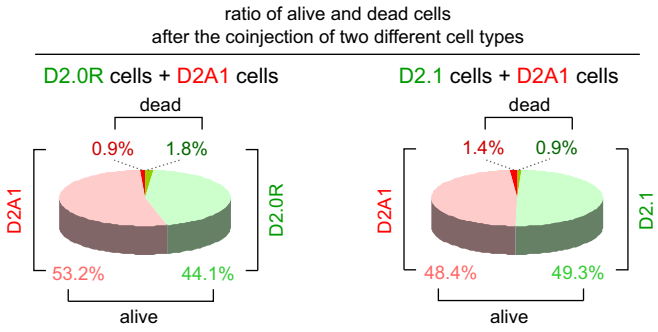

D

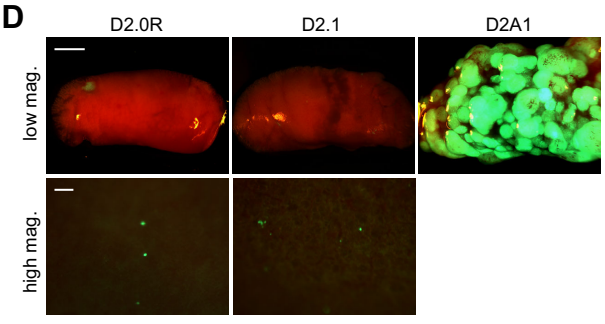

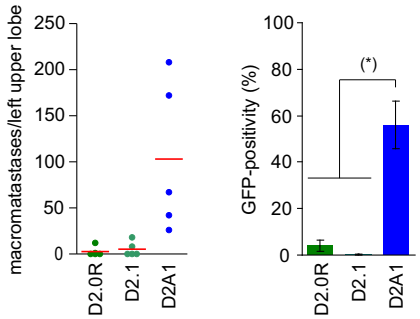

Supplementary Figure S1. Lung colonization by the various populations of D2 cells

(A) Summary of the *in vitro* and *in vivo* behaviors of the three different D2 cell populations. Indicated is the percent positivity of the proliferation- and apoptosis-markers. Under *in vitro* conditions, proliferation and apoptosis were analyzed by the anti-Ki67

immunostaining and terminal deoxynucleotidyl transferase-mediated dUTP nick end labeling (TUNEL), respectively; under *in vivo* conditions, these processes were examined by bromodeoxyuridine (BrdU) incorporation and cleaved-caspase-3-staining, respectively. Red numbers in the proliferation rates indicate that under MoT conditions *in vitro* and in the lungs *in vivo*, the proliferation-marker positivity of the D2A1 cells was significantly larger than the corresponding values of the D2.0R and D2.1 cells ($p < 0.02$ by Student's *t*-test). Note that we previously tested three-dimensional (3D) cultures using several different gel types, which included Matrigel, pure collagen I gels of several different concentrations, and a collagen I gel mixed with fibronectin (10). The aggressive D2A1 cells proliferated far more rapidly than the other two nonaggressive D2 cell populations in all the gel types we tested. Among these, Matrigel yielded the greatest difference, leading us to adopt the Matrigel-based MoT culture system for the present study. For extravasation, the relative abundance of extravasated cells at 48 hours after the coinjection of the aggressive D2A1 cells and either of the nonaggressive D2 cell types – D2.0R cells or D2.1 cells – is indicated. The number of extravasated D2A1 cells was set to 100. See B for the details of the method of extravasation measurement. Also see previous publications of us and others (7, 9, 10, 54).

(B) Extravasation of the nonaggressive and aggressive D2 cell types to the lung parenchyma following intravenous injection. Equal numbers of the nonaggressive D2.1 cells expressing membrane-targeted YPet (YPet-membrane; green) and the aggressive D2A1 cells expressing membrane-targeted tdTomato (tdTomato-membrane; red) were injected into mice through the tail vein. At indicated time points after the injection, lungs were harvested and frozen-sectioned, on which blood vessels (by PECAM-1 staining; white) and the nuclei (by Hoechst 33342 staining; blue) were visualized. Presented are the representative low and high magnification images of these sections (left). The regions marked in yellow color represent the lumina of the blood vessels. The relative abundance of cells remaining within the vascular lumina (intravascular) and extravasated cells, analyzed by direct counting on the sections, was plotted (far right). To determine whether the cells were extravasated or not, individual D2 cell and the surrounding lung microvasculature were examined at several different Z-positions. Cells of the other nonaggressive line, D2.0R – also expressing YPet-membrane – were also injected into mice together with the D2A1 cells expressing tdTomato-membrane, and the relative abundance of intravascular and extravasated cells was similarly plotted (second from right). (ns) $p > 0.1$ for both 'D2.0R (D2.1) intravascular cells vs D2A1 intravascular cells' and 'D2.0R (D2.1) extravasated cells vs D2A1 extravasated cells'.

(C) Apoptosis of the D2 cells within the lung tissue following tail-vein injection. D2 cells were labeled with fluorescent proteins and the two different cell types were co-injected through the tail vein as in B. 48 hours later, frozen sections of the lung tissue were prepared, in which apoptotic cells (by cleaved-caspase-3 staining; white) and the nuclei (blue) were visualized (left). The relative abundance of dead and alive cells was plotted (right).

(D) Lung metastasis formation after tail-vein injection of D2 cells. Lungs were harvested 24 days after the injection of GFP-labeled D2 cells. Representative low and high magnification images of the lungs were presented (left). The numbers of macroscopic metastases observed on the surface of left upper lobe of the lungs were plotted (middle). The red horizontal bar indicates the mean value in each sample population. GFP-positivity of cells in the lungs was analyzed by flow cytometry (right).

(E) Primary tumor formation by the D2 cells following orthotopic implantation. Three different populations of D2 cells were implanted into the mammary fat pads of mice, and the incidence and the weight of primary tumors were scored subsequently. Tumor incidence was evaluated by the formation of palpable tumors within 7 weeks of implantation. (*) $p < 0.01$.

Bars = 100 μm (B [low mag.], C, D [high mag.]), 20 μm (B [high mag.]), 2 mm (D [low mag.]). Values = means ± SD ($n = 4$; B, $n = 5$; D), means ± SEM ($n \geq 6$; E).

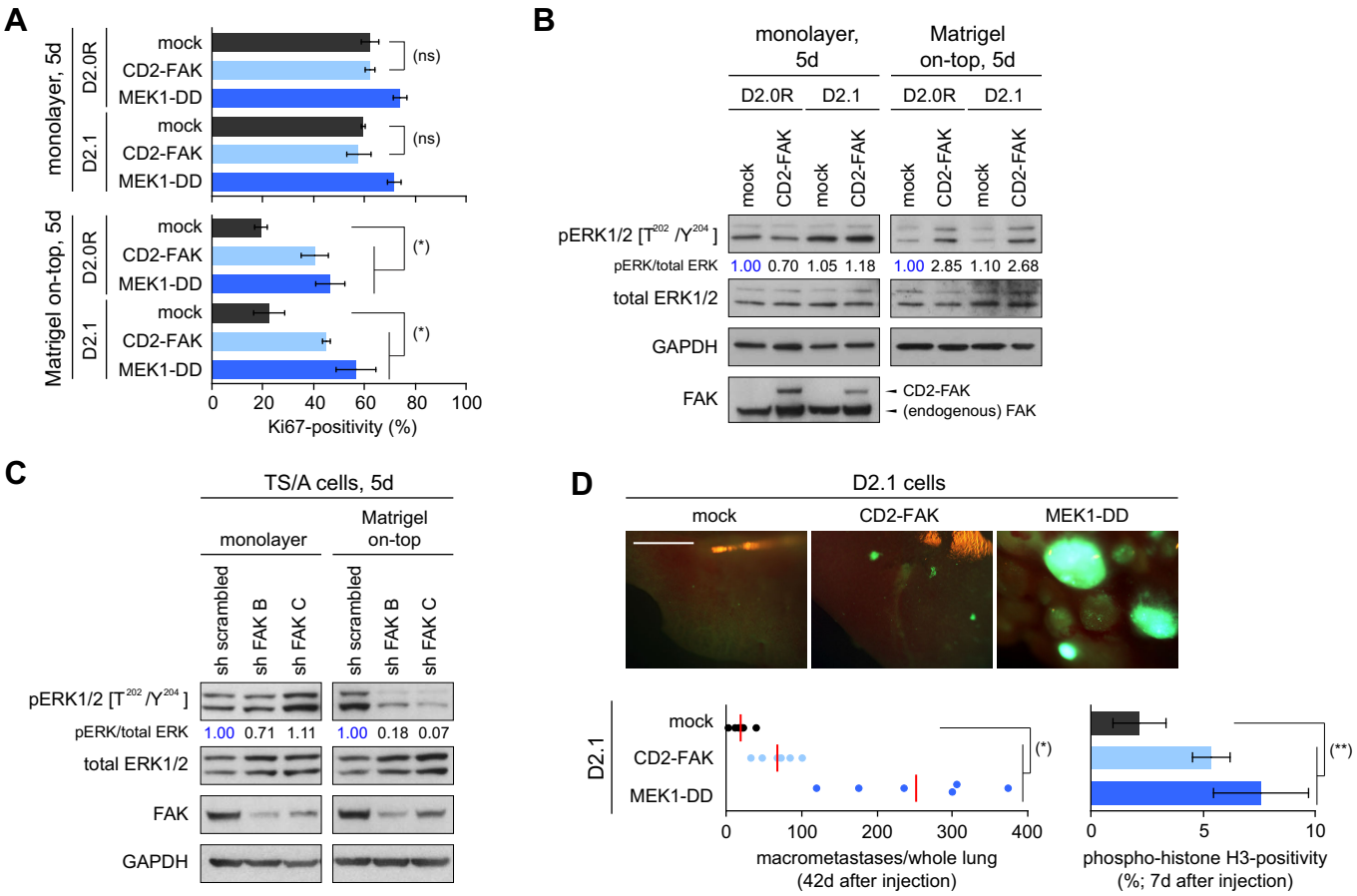

Supplementary Figure S2. Connection of FAK/ERK signaling and cell proliferation in various cell types

(A) *In vitro* proliferation of the otherwise-indolent D2.0R and D2.1 cells following enforced activation of the FAK/ERK signaling. The effects of expressing the constitutively active form of either FAK or MEK1 (CD2-FAK and MEK1-DD, respectively) were tested. Under MoT culture conditions, both CD2-FAK and MEK1-DD restored the proliferation of the otherwise-slowly proliferating D2.0R and D2.1 cells. (ns) $p > 0.5$, (*) $p < 0.01$.

(B) Phosphorylation of ERKs in the D2.0R and D2.1 cells following enforced activation of FAK. Under the MoT conditions of culture, ectopic expression of the constitutively active CD2-FAK fusion protein in the otherwise-indolent D2.0R and D2.1 cells sufficed to enhance the phosphorylation of ERKs. In contrast, the expression of CD2-FAK did not noticeably affect the phosphorylation levels of ERKs when these cells were growing as a monolayer.

(C) Role of FAK in ERK phosphorylation in the *in vitro* cultured TS/A cells. The knockdown of FAK expression strongly reduced the phosphorylation levels of the ERKs under the MoT culture conditions; in contrast, ERK phosphorylation levels were not noticeably affected by FAK knockdown when the TS/A cells were growing under monolayer culture conditions. This mirrored the condition-dependent effect of FAK knockdown on the levels of ERK phosphorylation observed in another metastatic cell line, D2A1 (see Fig. 1A). Together, these observations indicated that under certain conditions, such as MoT culture conditions *in vitro* and within the lung parenchyma *in vivo*, multiple types of metastatic cells rely on FAK signaling for efficiently activating the ERKs.

(D) *In vivo* behaviors of the D2.1 cells following enforced activation of the FAK/ERK signaling. D2.1-GFP cells, also expressing constitutively active forms of FAK (CD2-FAK) or MEK1 (MEK1-DD), or the control vector (mock), were tested for lung metastasis formation (top, bottom-left) following tail-vein injection into mice. The proliferation rates of the manipulated D2.1 cells within the lung tissue were also determined (bottom-right). (*) $p < 0.005$, (**) $p < 0.03$. Both CD2-FAK and MEK1-DD sufficed to confer the ability to proliferate rapidly in the lungs and thus to colonize the lung tissue efficiently on the otherwise-indolent D2.1 cells. Bar = 1 mm. The red vertical bar represents the mean value in each sample group.

To determine the ratio of band intensities (pERK/total ERK; B,C), the intensities of the bands of phospho-ERK1/2 blot were first normalized against the intensity of the corresponding bands of total ERK1/2 blot. Subsequently, the values relative to that of the sample of D2.0R-mock (B) or TS/A-sh scrambled (C) cells were calculated.

Values = means ± SD ($n = 3$; A,D).

A

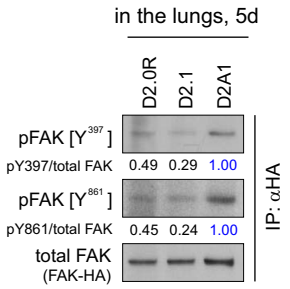

B

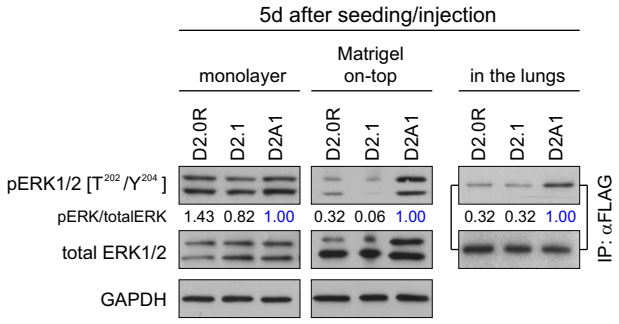

C

summary of the behaviors (FAK/ERK activation and proliferation) of the nonaggressive D2.0R/D2.1 cells and the aggressive D2A1 cells under various conditions

monolayer		Matrigel on-top (MoT)/ within the lung parenchyma
Y397 phosphorylation: D2.0R, D2.1 ≒ D2A1 (< 2-fold difference in band intensity) Y861 phosphorylation: D2.0R, D2.1 < D2A1 (≥ 4-fold difference in band intensity)	FAK activation (phosphorylation on Y397, Y861)	both Y397 and Y861 phosphorylation: D2.0R, D2.1 < D2A1 (> 4-fold difference in band intensity) [MoT] (> 2-fold difference in band intensity) [lung]
FAK signaling is not nessesary for ERK acvtivation FAK knockdown did not discernibly affect (< 1.5-fold change in band intensity) ERK phosphorylation levels in the D2A1 cells	role of FAK in ERK activation	FAK signaling is both nessesary and sufficient for ERK acvtivation FAK knockdown reduced (> 2.5-fold decrease in band intensity) ERK phosphorylation levels in the D2A1 cells [MoT, lung] CD2-FAK expression stimulated (> 2-fold increase in band intensity) ERK phosphorylation levels in the D2.0R/D2.1 cells [MoT only]
D2.0R, D2.1 ≒ D2A1 (< 1.5-fold difference in band intensity)	ERK activation (phosphorylation on T202/Y204 [ERK1], T185/T187 [ERK2])	D2.0R, D2.1 < D2A1 (> 3-fold difference in band intensity) [MoT, lung]
D2.0R, D2.1 ≒ D2A1 (Ki67 positvity in these cell types was 59.7%, 62.3% and 64.6%, respectively.)	proliferation rate	D2.0R, D2.1 < D2A1 (Ki67 positvity in these cell types was 17.2%, 16.6% and 71.2% [MoT], while the positivity of BrdU incorporation was 4.3%, 5.9% and 37.4% [lung], respectively.)

Supplementary Figure S3. Activation status of FAK and ERKs in the three different D2 cell populations

(A) The phosphorylation of FAK within the D2 cells disseminated in the lung parenchyma. Three different populations of D2 cells, all expressing HA-tagged FAK (FAK-HA), were injected into mice through the tail vein. Subsequently, the lung tissue was harvested, minced and lysed. FAK-HA was immunoprecipitated from the lysate and analyzed by immunoblotting. The ratio of band intensities (pFAK/total FAK) relative to that of the D2A1 cells is indicated. In a previous study, we similarly determined the ratio of band intensities in the blots of the samples prepared from the *in vitro* cultured D2.0R, D2.1 and D2A1 cells; these were 0.51, 0.83 and 1.00 (for D2.0R, D2.1 and D2A1, respectively; pFAK [Y^{397}] blot, monolayer culture conditions), 0.01, 0.25 and 1.00 (pFAK [Y^{861}] blot, monolayer culture conditions), 0.24, 0.18 and 1.00 (pFAK [Y^{397}] blot, MoT culture conditions), and 0.13, 0.10 and 1.00 (pFAK [Y^{861}] blot, MoT culture conditions) (10).

(B) ERK phosphorylation in the D2 cells under various conditions. As in Fig. 1A, D2 cells expressing the FLAG-ERK protein were used for determining ERK phosphorylation levels following the dissemination of these cells within the lung tissue. FLAG-ERK precipitated form the lung lysate was analyzed. The ratio of band intensities (pERK/total ERK) relative to that of the D2A1 cells is indicated.

(C) Summary of the activation status of FAK/ERK signaling and the rate of proliferation in the D2 cells under various conditions. This is based on the results shown in Fig. 1, Supplementary Figs. S2 and S3 as well as those presented in our previous publication (10).

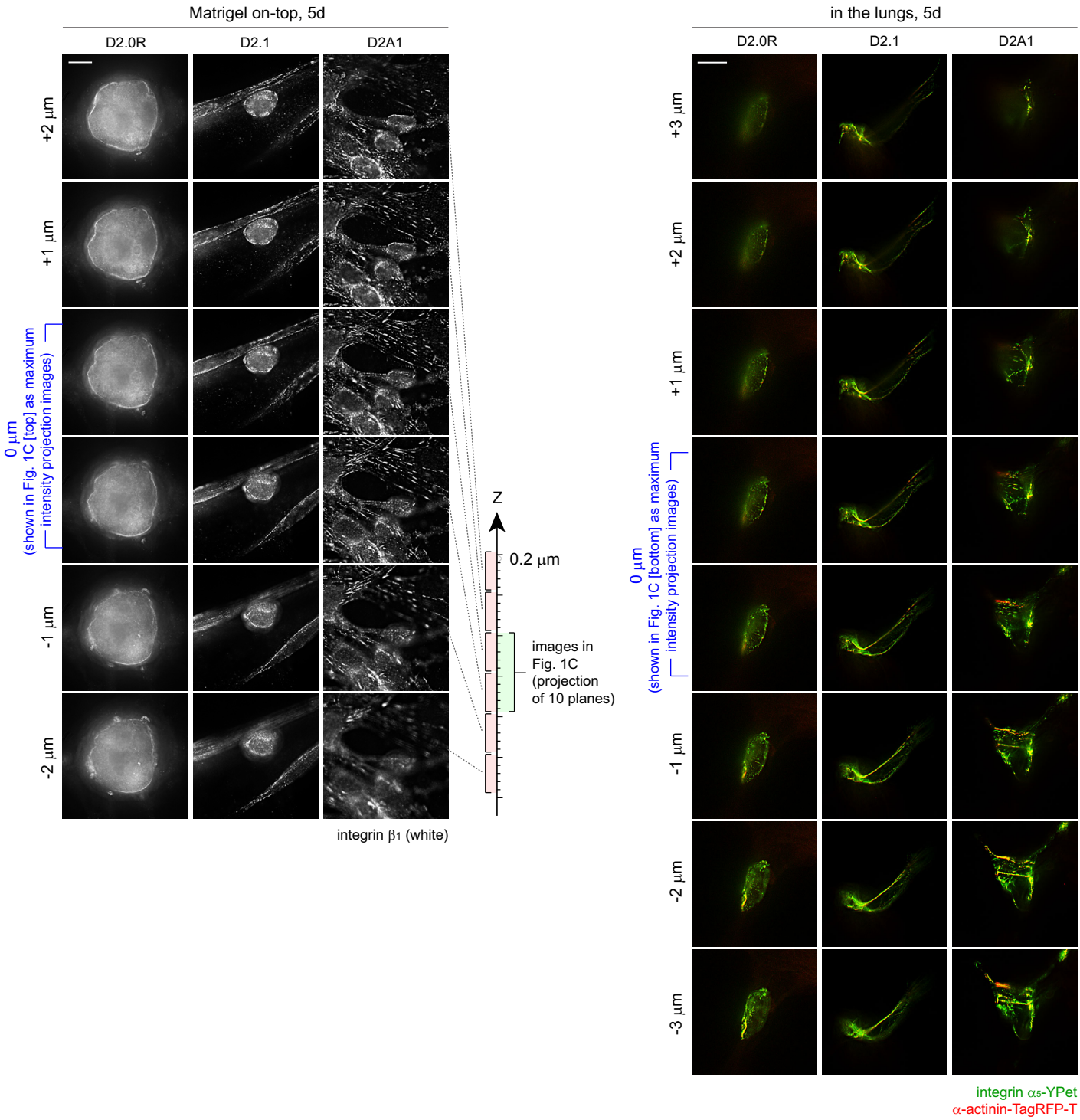

Supplementary Figure S4. Z-section images of the elongated adhesion plaques formed by the aggressive D2A1 cells

Z-section images associated with the micrographs of MoT-cultured cells (left) and the cells residing in the lung tissue (right) shown in Fig. 1C. For these micrographs, images taken from several different Z-positions are presented. Note that each image presented here represents the maximum intensity projection of 5 consecutive focal planes, surrounding the indicated Z-position, with a step size of 0.2 μm (see the ruler shown in the left panel), while the original images presented in Fig. 1C represent the maximum intensity projection of 10 consecutive focal planes. In the images shown in the right panel, green color represents the distribution of integrin α_5-YPet, whereas red color represents that of α-actinin-Tag-RFP-T.

Bars = 10 μm.

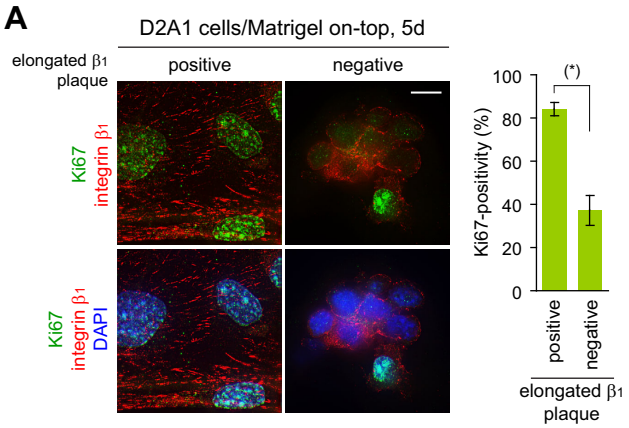

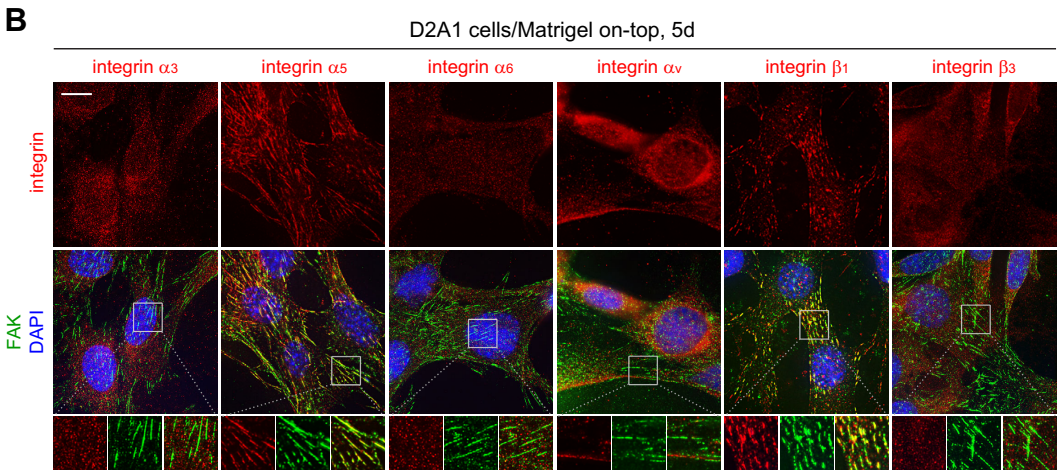

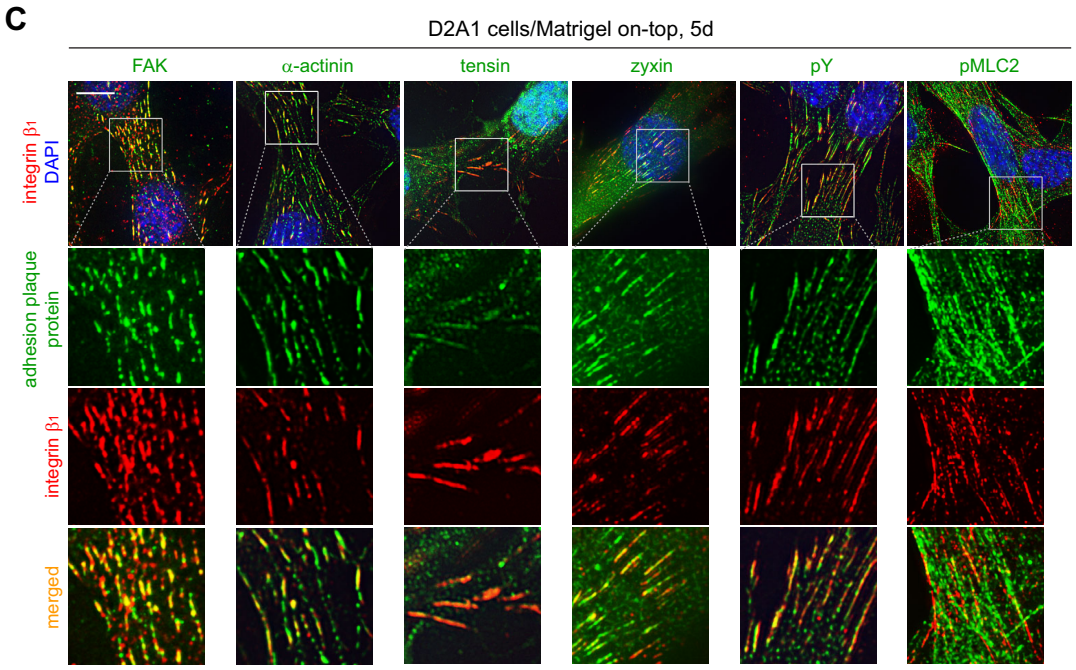

Supplementary Figure S5. Detailed characterization of elongated adhesion plaques formed under MoT conditions

(A) Correlation between elongated adhesion plaque formation and proliferation. D2A1 cells were propagated under the MoT conditions of culture for 5 days and stained for Ki67 (green), integrin β_1 (red) and nuclei (blue) (left). These cells were divided into two subgroups by the representation of elongated β_1 plaques (see Supplementary Methods). The positivity of nuclear Ki67 staining within these subgroups was plotted (right). (*) $p = 0.002$. Values = means ± SD ($n = 3$). This tight correlation between the assembly of integrin β_1-

containing, elongated forms of adhesion plaques and the rate of proliferation provided additional support for the notion that the formation of such plaque contributed functionally to the proliferation of these cells (also see main text).
(B) Subcellular localization of various integrin subunits in MoT-cultured D2A1 cells. D2A1 cells were cultured under MoT conditions for 5 days and stained for integrin subunits (α_3, α_5, α_6, α_v, β_1 and β_3; red), FAK (green) and nuclei (by DAPI; blue). Among the integrin subunits tested, only integrin α_5 and β_1 accumulated to the elongated adhesion plaques and thereby colocalized with FAK within these structures.
(C) Localization of various adhesion plaque proteins to the elongated adhesion plaques formed in MoT-cultured D2A1 cells. D2A1 cells were cultured under MoT conditions for 5 days and stained for adhesion plaque proteins (FAK, α-actinin, tensin and zyxin; green), integrin β_1 (red) and nuclei (by DAPI; blue). In cells forming a monolayer, tensin and zyxin are not initially recruited to sites of adhesion but subsequently accumulate in adhesion plaques as these plaques develop a mature morphology (55). Hence, the elongated adhesion plaques observed in MoT-cultured D2A1 cells have a subunit composition similar to that of mature adhesion plaques observed by others in monolayer-forming cells. Phosphotyrosine-containing proteins (green; second from right) were also enriched within these elongated adhesion plaques, indicating the presence of active signaling events associated with these plaques. We also analyzed the localization of myosin light chain 2 phosphorylated on serine 19 (pMLC2); the phosphorylation of MLC2 on this residue serves as an indicator of actomyosin contractility (56). pMLC2 localization was overlapped partly with that of integrin β_1, indicating the presence of contractile tension placed on these integrin β_1-containing, elongated adhesion plaques. However, pMLC2 was also distributed out of these plaques, displaying filament-like patterns of localization. This suggested that pMLC2 was distributed along the entire lengths of actin stress fibers in MoT-cultured D2A1 cells, as observed previously by others in cells forming a monolayer (57).
Bars = 10 μm.

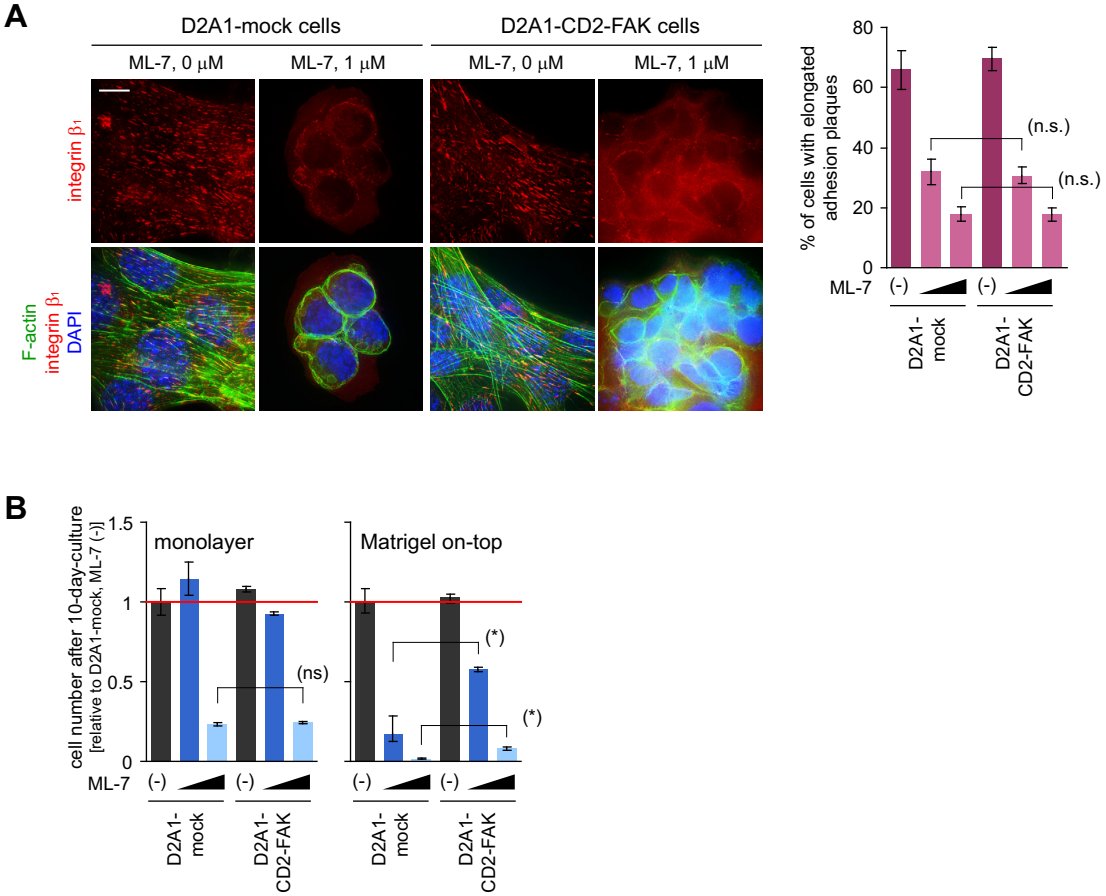

Supplementary Figure S6. Blocking adhesion plaque formation and proliferation by the functional inhibition of myosin II

(A) Essential role of myosin II in the formation of elongated adhesion plaques. The control (mock) and CD2-FAK-expressing D2A1 cells were propagated *in vitro* under MoT conditions of culture; these cells were grown for 5 days in the presence of the various concentrations of myosin light chain kinase (MLCK) inhibitor ML-7 (Sigma-Aldrich; 0 μM, 1 μM and 3 μM; also in B), which inhibits MLCK-dependent phosphorylation of the myosin II light chain and thereby blocks myosin II-mediated contractility. These cells were subsequently stained for integrin β_1 (red), F-actin (green) and nuclei (by DAPI; blue) (left). The presence of integrin β_1-containing, elongated adhesion plaques within each cell population was quantified (right). ML-7 treatment impaired the formation of integrin β_1-containing, elongated adhesion plaques in the D2A1 cells, which was consistent with a previously reported observation by others (9). This indicated the critical role of myosin II-mediated contractility in the development of these plaques. The expression of constitutively active CD2-FAK failed to rescue the formation of these plaques. Hence, while the assembly of integrin β_1-containing, elongated adhesion plaques served as a critical regulator of FAK activation (see main text), the enforced activation of FAK did not stimulate the formation of these plaques in the absence of myosin II activity. Bar = 10 μm.

(B) Essential role of myosin II in cell proliferation under MoT culture conditions. The manipulated D2A1 cells described in A were propagated *in vitro* for 10 days either as a monolayer or under MoT conditions of culture: here again, these cells were grown in the presence of the various concentrations of ML-7. The resulting cell number, relative to that of the D2A1-mock cells without ML-7 treatment, was plotted. (ns) $p > 0.2$, (*) $p < 0.02$. ML-7 treatment reduced the rate of proliferation under both culture conditions; however, this antiproliferative effect of ML-7 was more clearly observed under MoT conditions than in monolayer culture. This, when taken together with the result shown in A, indicated that myosin II activity was critical for the D2A1 cells to develop abundant, integrin β_1-containing adhesion plaques under MoT conditions of culture, which, in turn, contributed in an important way to the proliferation of these cells. CD2-FAK expression partly rescued the proliferation of ML-7-treated D2A1 cells specifically under MoT conditions of culture, while the expression of this fusion protein failed to restore the formation of integrin β_1-containing, elongated adhesion plaques in these cells (see A). This provided further support for the notion that FAK activation is a key intermediary that connects the assembly of elongated adhesion plaques and promotion of cell proliferation, but is not an upstream controller of the formation of such plaques.
Values = means ± SD (n = 3).

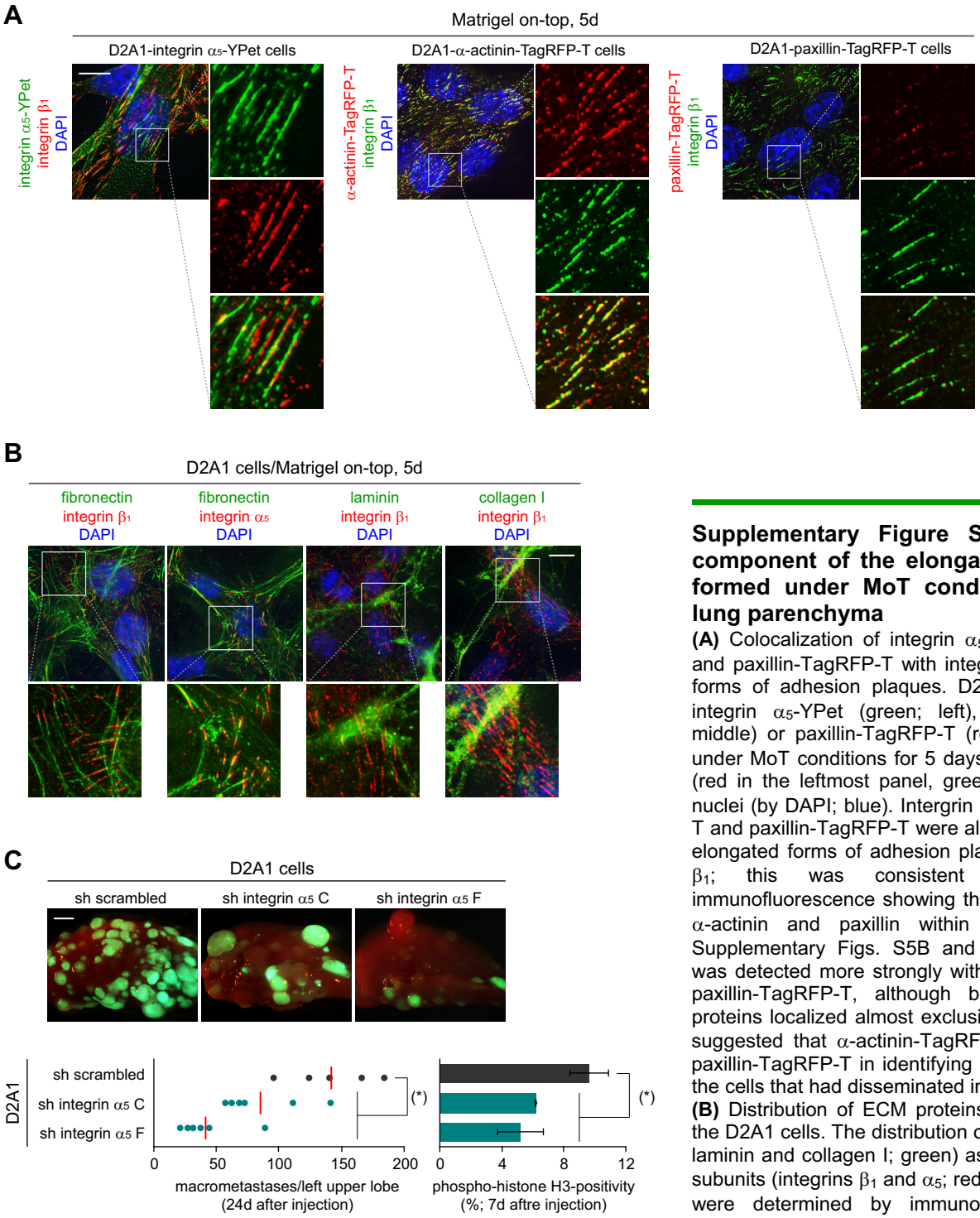

Supplementary Figure S7. Integrin α_5 as a component of the elongated adhesion plaques formed under MoT conditions and within the lung parenchyma

(A) Colocalization of integrin α_5-YPet, α-actinin-TagRFP-T and paxillin-TagRFP-T with integrin β_1 within the elongated forms of adhesion plaques. D2A1 cells expressing either integrin α_5-YPet (green; left), α-actinin-TagRFP-T (red; middle) or paxillin-TagRFP-T (red; right) were propagated under MoT conditions for 5 days and stained for integrin β_1 (red in the leftmost panel, green in right two panels) and nuclei (by DAPI; blue). Intergrin α_5-YPet, α-actinin-TagRFP-T and paxillin-TagRFP-T were all found to accumulate to the elongated forms of adhesion plaques together with integrin β_1; this was consistent with the results of immunofluorescence showing the localization of integrin α_5, α-actinin and paxillin within these plaques (ref. 10; Supplementary Figs. S5B and S5C). α-actinin-TagRFP-T was detected more strongly within these plaques than was paxillin-TagRFP-T, although both of these two fusion proteins localized almost exclusively to these plaques. This suggested that α-actinin-TagRFP-T was more useful than paxillin-TagRFP-T in identifying similar adhesion plaques in the cells that had disseminated into the lung tissue *in vivo*.

(B) Distribution of ECM proteins under the MoT culture of the D2A1 cells. The distribution of ECM proteins (fibronectin, laminin and collagen I; green) as well as that of the integrin subunits (integrins β_1 and α_5; red) and nuclei (by DAPI; blue) were determined by immunofluorescence. Integrin β_1-containing, elongated forms of adhesion plaques, observed in the MoT-cultured D2A1 cells, were aligned with fibronectin (left), but not laminin nor collagen I (second from right and rightmost, respectively). Moreover, integrin α_5, an integrin subunit that is paired exclusively with integrin β_1 to form major fibronectin receptor, was also found to accumulate to these plaques (second form left, also see Supplementary Fig. S5B). These observations, when taken together with the minute concentration of fibronectin contained within Matrigel, suggested that D2A1 cells secrete fibronectin to which they can then adhere via the $\alpha_5\beta_1$ integrin.

(C) Contribution of integrin α_5 to the proliferation of cancer cells disseminated to the lung tissue. The control (sh scrambled) and integrin α_5-knockdown (sh integrin α_5 C and F: two different sh RNA sequences targeting integrin α_5 were tested) D2A1 cells were injected into mice via the tail vein and subsequent metastasis formation in the lungs was analyzed (top, bottom-left). The proliferation rates of these manipulated D2A1 cells within the lung tissue were also determined (bottom-right). Values = means ± SD (n = 3; middle). In the bottom-left graph, the red vertical bar represents the mean value in each sample group. (*) $p < 0.05$.

Bars = 10 μm (A,B), 2 mm (C).

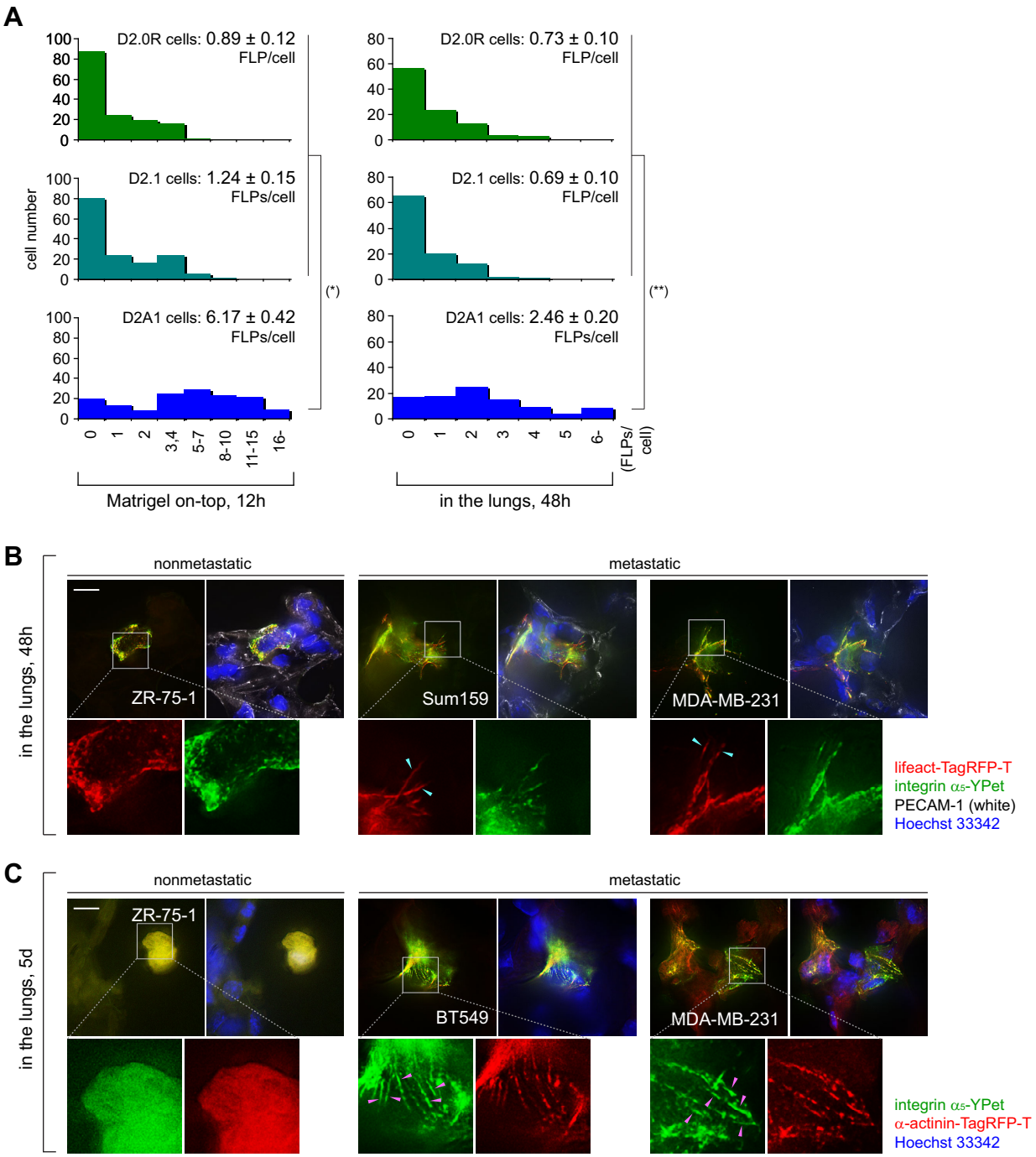

Supplementary Figure S8. FLPs formed specifically by metastasis-competent cells under MoT conditions and within the lung parenchyma

(A) The formation of FLPs by the various D2 cell populations under MoT culture conditions and within the lung parenchyma. The number of FLPs per cell observed under these conditions was presented as histograms. Values = means ± SEM (n = 150 [MoT], 100 [lungs]). (*) $p < 1 \times 10^{-21}$, (**) $p < 1 \times 10^{-11}$. See also Figs. 2D and 2E.

(B) FLP formation by the human breast cancer cell lines *in vivo*. These cell lines were manipulated to express integrin α_5-YPet (green) and lifeact-Tag-RFP-T (red) and injected into mice through the tail vein. These images supplement the result shown in Fig. 3C.

(C) Elongated adhesion plaque formation by the human breast cancer cell lines *in vivo*. These cell lines were manipulated to express integrin α_5-YPet (green) and α-actinin-Tag-RFP-T (red) and injected into mice through the tail vein. These images supplement the result shown in Fig. 3D.

Bars = 10 μm (B,C).

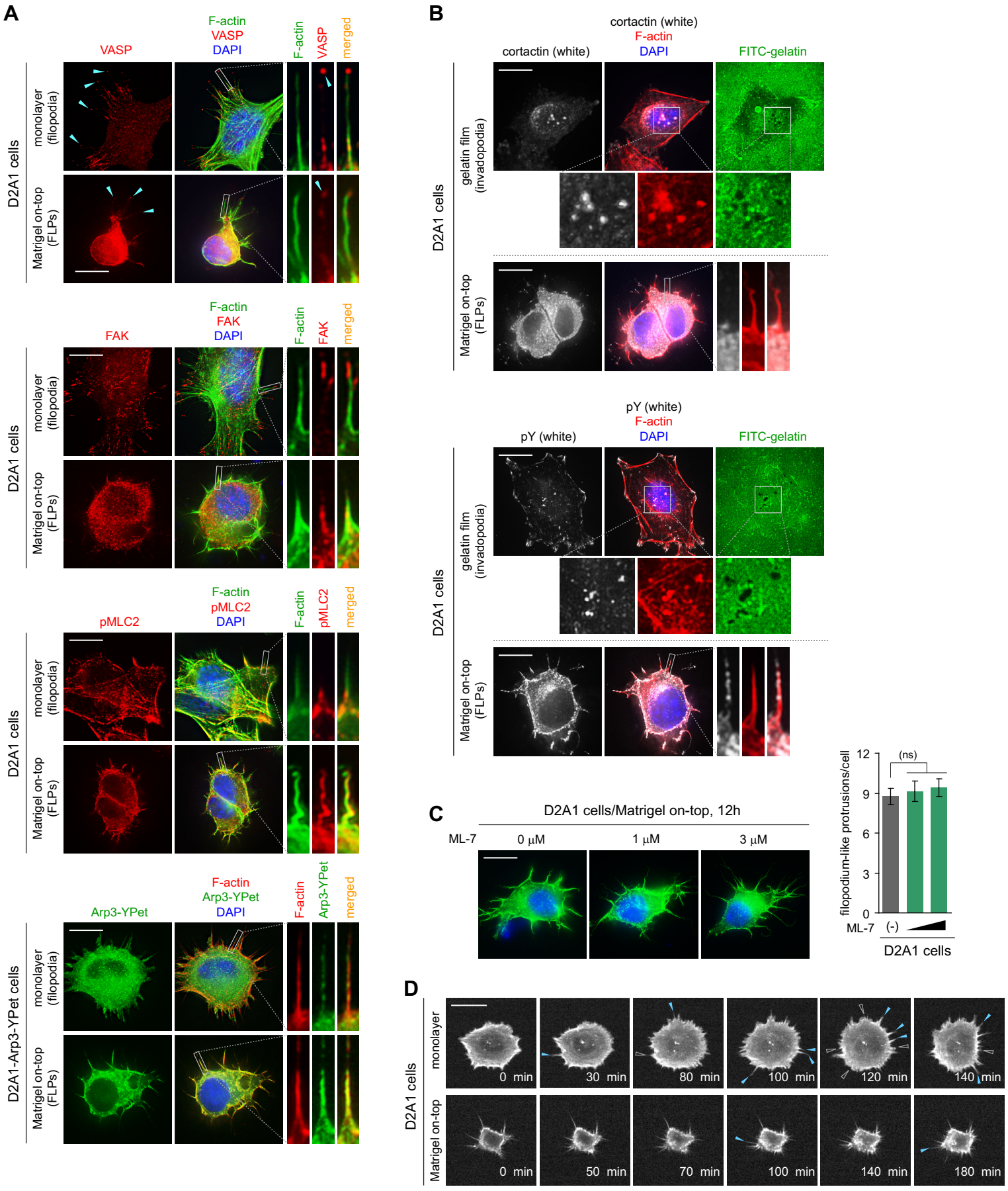

Supplementary Figure S9. Detailed characterization of FLPs formed by the MoT-cultured D2A1 cells

(A) Further comparison of the two types of protrusions, filopodia in monolayer-forming cells and FLPs in MoT-cultured cells. D2A1 cells were cultured either as a monolayer on laminin- and collagen I-coated glass plates or under MoT conditions for 4 and 12 hours,

respectively. These cells were subsequently stained for F-actin (green) and nuclei (by DAPI; blue), as well as for other potential components of these protrusions (red), including vasodilator-stimulated phosphoprotein (VASP), FAK and MLC2 phosphorylated on serine 19 (pMLC2) (top three panels). To detect the localization of Arp3, a component of the Arp2/3 actin-organizing complex, D2A1 cells expressing the Arp3-YPet fluorescent fusion protein were also propagated either as a monolayer or under MoT conditions; these cells were also subject subsequently to F-actin (red) and nuclei (blue) staining (bottom panel). VASP was enriched at the tips of both filopodia and FLPs; the majority (> 70%) of both types of protrusions displayed the tip-specific stainings of VASP (blue arrowheads). FAK was enriched at the tips of filopodia extending from monolayer-forming cells, while this kinase was distributed evenly along the lengths of the shafts of FLPs in MoT-cultured cells. The differing patterns of FAK distribution in these two different types of protrusions echoed the distribution patterns of integrin β_1 (see Fig. 4A). pMLC2 was enriched at the roots of filopodia, but was distributed evenly along the entire lengths of FLPs. Finally, the Arp3-YPet fusion protein exhibited only weak distribution to filopodial shafts, while this fusion protein was strongly detected along the entire lengths of the shafts of FLPs. These observations, when taken together with the results shown in Figs. 4A and 4B, revealed the common and different structural traits between filopodia and FLPs.

(B) The comparison of invadopodia and FLPs. For invadopodium formation, D2A1 cells were cultured on top of a film of FITC-labeled gelatin for 7 hours (see Supplementary Methods), whereas these cells were propagated under MoT conditions for 12 hours for the formation of FLPs. Invadopodia were identified as F-actin accumulations associated with the degradation of gelatin film (marked by the loss of FITC fluorescence [green]). Cells cultured on these gelatin films as well as those propagated under MoT conditions were stained for F-actin (red), invadopodium markers (cortactin and tyrosine-phosphorylated proteins [pY]; white), and the nuclei (blue). Both invadopodia and FLPs contained abundant tyrosine-phosphorylated proteins, while FLPs did not harbor cortactin – a marker for invadopodia; this indicated that the composition of FLPs differed from that of invadopodia.

(C) Dispensable role of myosin II in the formation of FLPs. D2A1 cells were propagated under MoT conditions for 12 hours in the presence of the various concentrations of myosin light chain kinase inhibitor, ML-7 (0 μM, 1 μM and 3 μM)). Subsequently, cells were stained for F-actin (green) and nuclei (by DAPI; blue) (left). The number of FLPs per cell within each cell population was plotted. FLPs formed in the presence of ML-7 appeared to be thinner and longer than those formed in the absence of this inhibitor; however, ML-7 treatment did not significantly alter the number of FLPs per cell. This indicated that the activity of myosin II is dispensable for the extension of FLPs, which contrasted sharply with the critical involvement of myosin II-mediated contractility for the subsequent assembly of elongated, mature adhesion plaques (see Supplementary Fig. S6A). (ns) $p > 0.4$. Values = means ± SEM ($n = 100$).

(D) The kinetics of the assembly and disassembly of filopodia and FLPs. D2A1 cells expressing the lifeact-YPet fluorescent actin marker were propagated either as a monolayer or under MoT conditions of culture, where the assembly and disassembly of filopodia and FLPs were analyzed by time-lapse microscopy. Shown are the representative image series of cells growing under each of these conditions. The formation of new filopodia (or FLPs) is indicated by the blue filled arrowheads, whereas the disappearance of previously existed filopodia (or FLPs) is indicated by the gray open arrowheads. See also Fig. 4C, Supplementary Movies S1 and S2.

Bars = 10 μm.

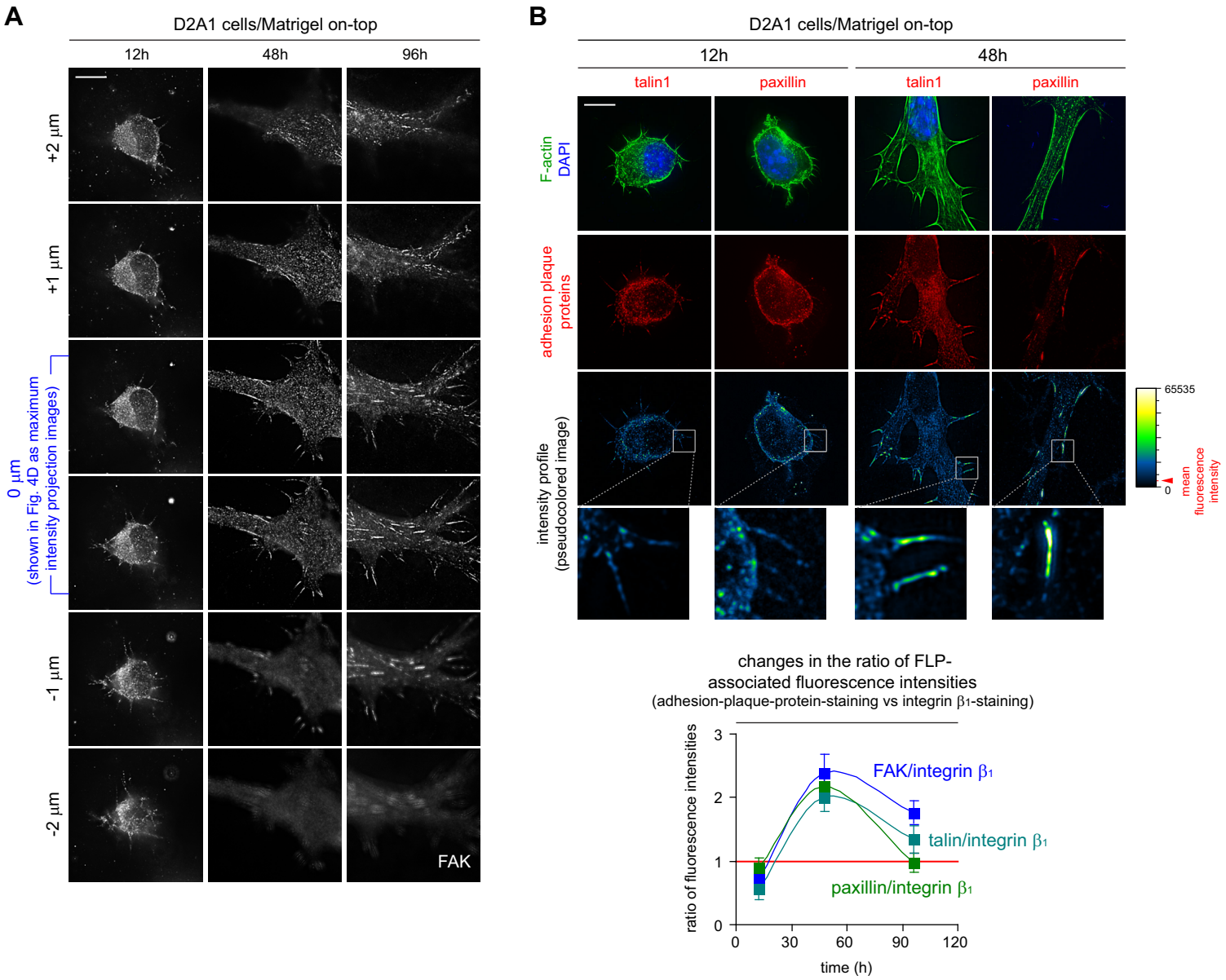

Supplementary Figure S10. FLPs as initial sites for the accumulation of adhesion plaque proteins

(A) Z-section images associated with the micrographs of FAK staining shown in Fig. 4D. For these micrographs, images taken from several different Z-positions (+2 μm, +1 μm, 0 μm, -1 μm and -2 μm relative to the original images) are presented.

(B) Accumulations of FAK, talin1 and paxillin to FLPs and elongated adhesion plaques. The localization of F-actin (green), nuclei (blue) and either of talin1 and paxillin (red) was determined in the D2A1 cells that were propagated under MoT conditions for the indicated time periods (top). These images supplement the results shown in Fig. 4D. In addition, the ratio of the intensities of FLP-associated fluorescence, between that of adhesion plaque protein (FAK, talin1 or paxillin) staining and that of integrin β_1 staining, was plotted (bottom). Values = means ± SEM ($n \fallingdotseq 30$). Note that the amount of integrin β_1 protein associated with FLPs was relatively constant during the course of the observation period (Fig. 4D). These various observations, when taken together, revealed that FLPs initially harbored small amounts of adhesion plaque proteins (FAK, talin1 and paxillin) relative to the amount of integrin β_1 that they contained. These adhesion plaque proteins accumulated subsequently to FLP-associated integrin β_1 (see changes between 12h and 48h). The ratio of adhesion plaque proteins to integrin β_1 went down again as cells started to develop abundant, elongated forms of adhesion plaques (changes between 48h and 96h); this was caused presumably by the selective translocation – from FLPs to elongated adhesion plaques – of the integrin β_1 protein that interacted with abundant adhesion plaque proteins. Hence, FLPs are likely to contribute to the formation of elongated, mature adhesion plaques by providing sites for the nucleation of protein complexes that constitute the core of these plaques. This, in turn, prompted us to postulate that FLPs formed in MoT-cultured cells are functionally equivalent to focal complexes that are developed near the edge of lamellipodia in cells growing under monolayer conditions; both of these structures serve as sites for the initial assembly of adhesion plaque proteins.

Bars = 10 μm.

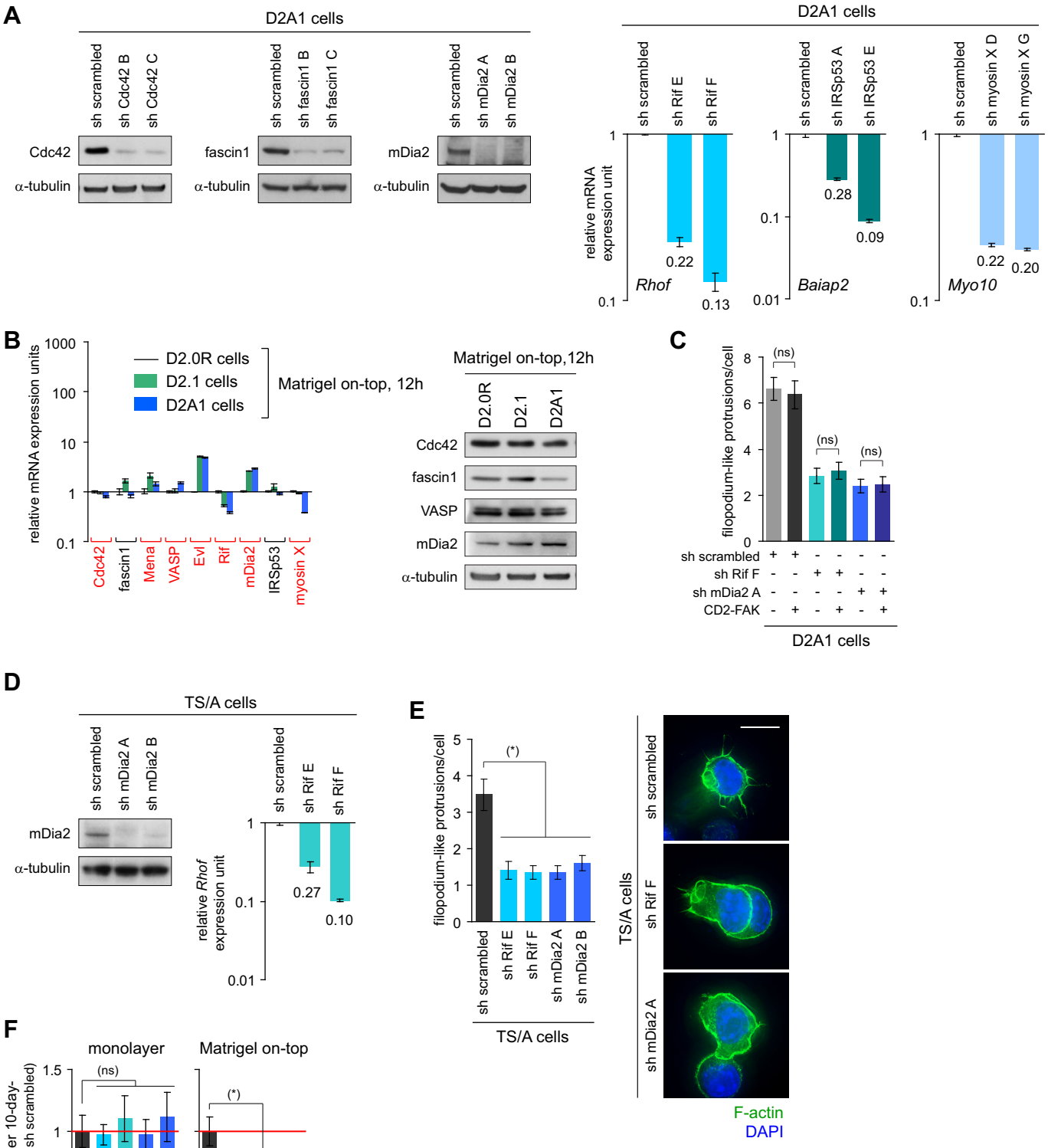

Supplementary Figure S11. The knockdown of the expression of potential FLP regulators

(A) Knockdown efficiency of Cdc42, fascin1, mDia2, Rif, IRSp53 and myosin X expression in the D2A1 cells. For Cdc42, fascin1 and mDia2 expression, the knockdown efficiency was assessed by immunoblotting, whereas RT-PCR was used to evaluate the knockdown efficiency of Rif mRNA: *Rhof*), IRSp53 (*Baiap2*) and myosin X (*Myo10*) expression.

(B) mRNA and protein expression of the candidate regulators of FLP formation. RNA and protein samples were prepared from the three different D2 cell populations that were propagated under MoT conditions of culture for 12 hours and analyzed by RT-PCR (left) and immunoblotting (right), respectively. In the graph showing the result of RT-PCR, red characters indicate *bona fide* regulators of FLP formation in the MoT-cultured D2A1 cells (see Fig. 5A). This result indicated that with the exception of mRNAs for mDia2 and VASP, the FLP-rich D2A1 cells showed even lower expression levels of the mRNAs encoding these FLP

regulators than did the poorly-FLP-forming D2.1 cells. Moreover, the protein expression levels of VASP and mDia2 proteins were comparable between the three different lines of D2 cells. These observations collectively indicated that the expression levels of the FLP regulators tested here did not account, by themselves, for the differing abundances of FLPs between the various D2 cell types. We also found, however, that the aggressive D2A1 cells exhibited the level of GTP-bound, active Cdc42 much higher (2.7 to 5.1 fold) than those observed in the more indolent D2.0R and D2.1 cells under the MoT conditions of culture (data not shown); this might account, at least in part, for the observed difference in the abundance of FLPs between these various D2 cell populations.

(C) Effect of CD2-FAK expression on the formation of FLPs. The control as well as Rif- or mDia2-knockdown D2A1 cells were further engineered to express CD2-FAK. These and the control cells were tested for the formation of FLPs. Plotted is the number of FLPs per cell within each cell population. CD2-FAK expression did not restore the formation of FLPs in the Rif-knockdown or mDia2-knockdown D2A1 cells. (ns) $p > 0.6$. This provided additional support for the notion that FAK is activated as a consequence of FLP extension and subsequent assembly of elongated adhesion plaques and does not have regulatory effects on the formation of FLPs and elongated adhesion plaques (see also Supplementary Fig. S6B).

(D) Knockdown efficiency of mDia2 and Rif expression in the TS/A cells. For mDia2, the knockdown efficiency was tested by immunoblotting, whereas RT-PCR was used to evaluate the knockdown efficiency of Rif expression.

(E) Involvement of Rif/mDia2 pathway in the formation of FLPs by TS/A cells growing under the MoT conditions. The control (sh scrambled), Rif-knockdown and mDia2-knockdown TS/A cells were propagated under MoT culture conditions for 12 hours and stained for F-actin (green) and the nuclei (by DAPI; blue) (right). The number of FLPs per cells within each cell population was plotted (left). (*) $p < 0.0002$. Bar = 10 μm.

(F) Essential role of Rif/mDia2 pathway in the proliferation of TS/A cells under MoT conditions. The control, Rif-knockdown and mDia2-knockdown TS/A cells were propagated either as a monolayer or under MoT conditions of culture for 10 days. The resulting cell number relative to that of the control cells, was plotted. (ns) $p > 0.4$, (*) $p < 0.01$.

Values = means ± SD ($n = 3$; A,B,D,F), means ± SEM ($n = 100$; C,E).

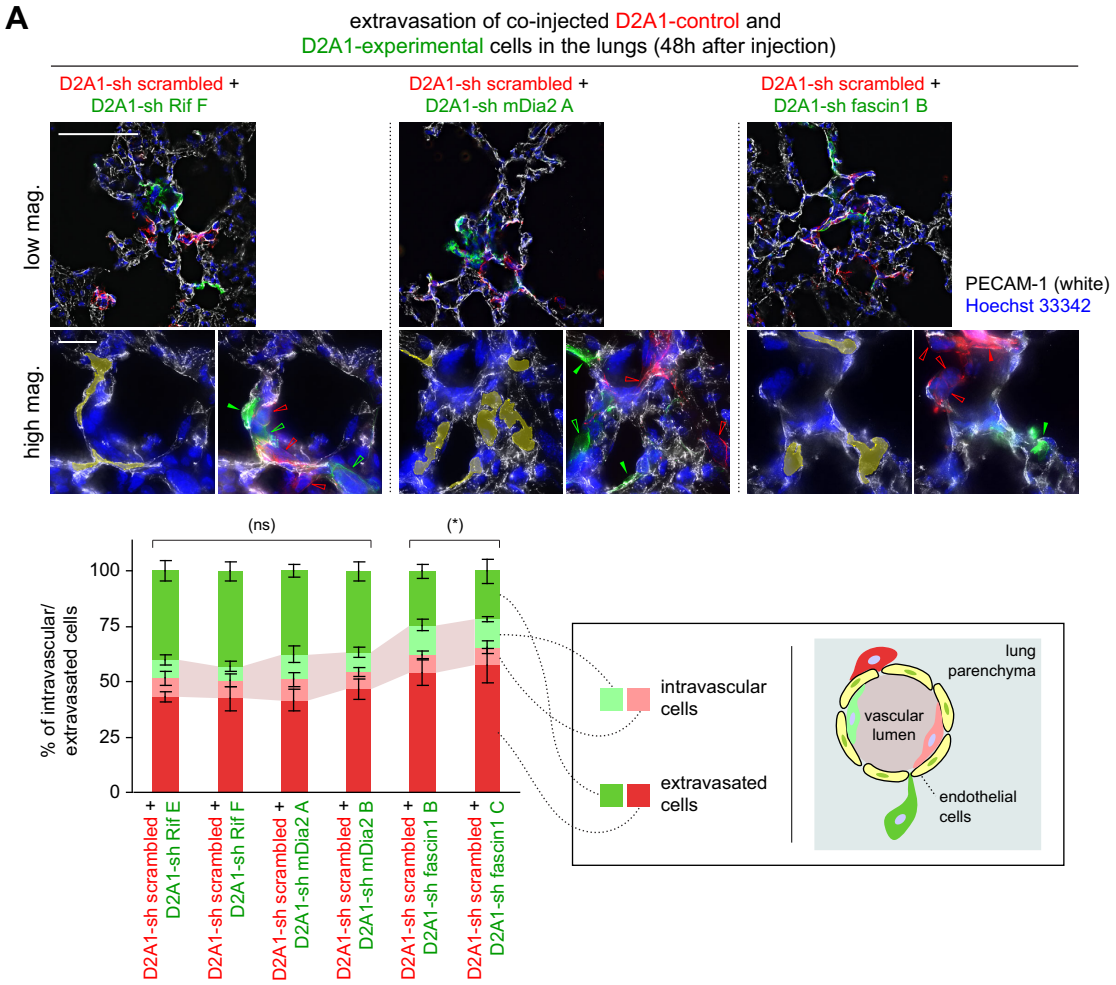

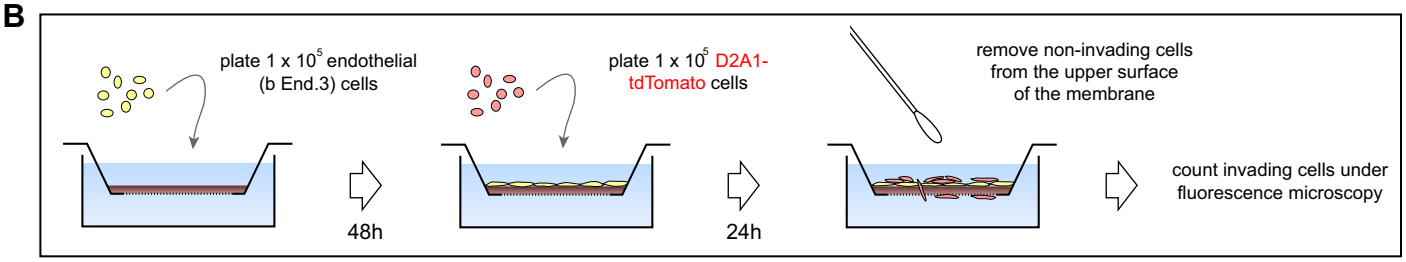

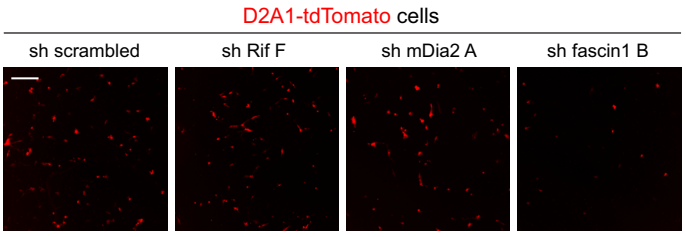

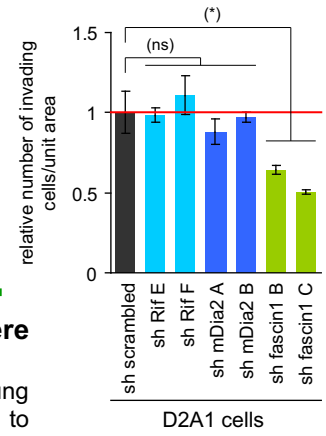

Supplementary Figure S12. Extravasation of the D2A1 cells that were manipulated to block FLP formation

(A) Effect of Rif-, mDia2- and fascin1-knockdown on extravasation into the lung parenchyma. Equal numbers of the control D2A1 cells (sh scrambled) engineered to express tdTomato-membrane (red) and Rif-, mDia2- or fascin1-knockdown D2A1 cells, also expressing YPet-membrane (green), were injected into mice through the tail vein. Extravasation of these cells to the parenchyma of the lungs was analyzed as in Supplementary Fig. S1B. Presented are the representative low and high magnification images of the lung sections, where blood vessels (by PECAM1-staining; white) and nuclei (by Hoechst33342; blue) were visualized (top). The regions marked in yellow color represent the lumina of the blood vessels. The relative abundance of cells

remaining within the vascular lumina (intravascular) and extravasated cells, was plotted (bottom). (ns) $p > 0.05$ for both 'D2A1-control (sh scrambled) extravasated cells vs D2A1-experimental extravasated cells' and 'D2A1-control intravascular cells vs D2A1-experimental intravascular cells'. (*) $p < 0.005$ for 'D2A1-control extravasated cells vs D2A1-experimental (sh fascin1) extravasated cells'. Being consistent with the previously reported role of fascin1 in trans-endothelial migration (58), the knockdown of facsin1 expression resulted in a 55-62 % decrease in the number of cells that successfully extravasated into the lung parenchyma 48 hours after the injection. In contrast, fascin1 knockdown minimally affected the formation of FLPs by the extravasated cells or on the post-extravasation proliferation of the D2A1 cells within the parenchyma of the lungs (Figs. 6A and 6D). Hence, the observed, modest effect of fascin1-knockdown on the development of macroscopic metastases by the D2A1 cells following tail-vein-injection (a 1.8 to 1.9 fold decrease in the number of macroscopic colonies; Fig. 6D) appears to be accounted for largely, if not entirely, by the inhibitory effect of this knockdown on the process of extravasation.

(B) Effect of Rif-, mDia2- and fascin1-knockdown on *in vitro* transendothelial migration. A confluent monolayer of endothelial cells (bEnd.3 cells) was formed on the Matrigel-coated membrane of Boyden chamber insert. The control (sh scrambled) and engineered D2A1 cells described in A, also expressing (cytoplasmic) tdTomato, were subsequently plated on top of the endothelial monolayer. Representative images of the membrane, following the removal of non-invading cells from the upper surface, were presented (left). The number of invading cells per unit area of the membrane, relative to the number of invading control cells, was plotted (right). (ns) $p > 0.2$, (*) $p < 0.04$.

Bars = 100 μm (A [low mag.]), 20 μm (A [high mag.]), 200 μm (B). Values = means ± SD ($n = 3$).

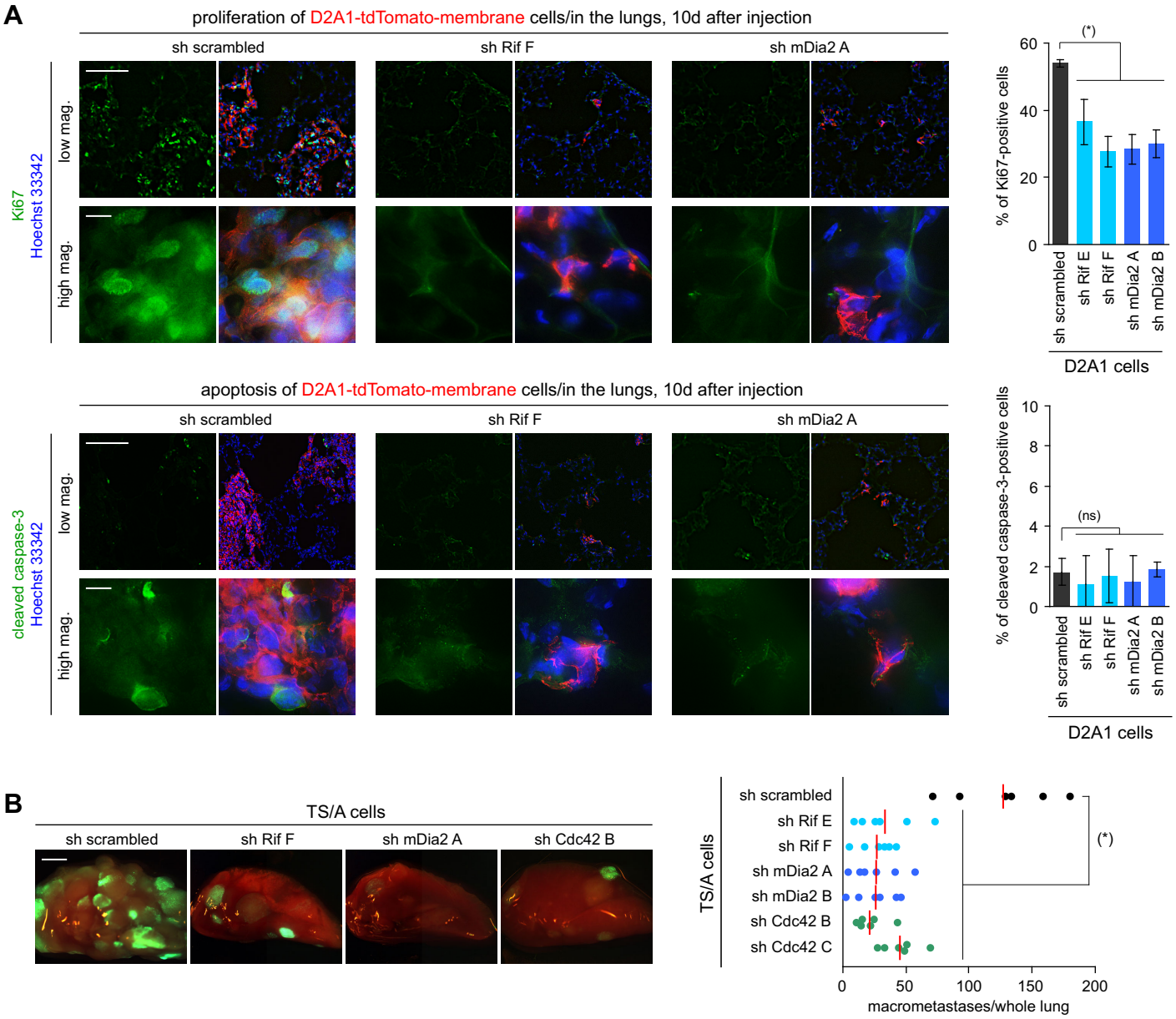

Supplementary Figure S13. Fate of the tail-vein-injected cells that were manipulated to block FLP formation

(A) Effect of Rif- and mDia2-knockdown on the proliferation and apoptosis of the D2A1 cells within the lung tissue. The control (sh scrambled), Rif-knockdown and mDia2-knockdown D2A1 cells, also expressing tdTomato-membrane, were injected into mice via the tail vein. 10 days later, lungs were harvested and frozen-sectioned. To analyze the proliferation and apoptosis of the D2A1 cells that had disseminated into the lung tissue, these sections were stained for the proliferation marker Ki67 (green; top) and the apoptosis marker cleaved caspase-3 (green; bottom), respectively, as well as for the nuclei (by Hoechst33342; blue) (left). The positivity of nuclear Ki67 staining and that of cytoplasmic cleaved caspase-3 staining within the populations of the D2A1 cells residing in the lung tissue were plotted (right). Notably, the majority (> 90%) of the cells constituting the micrometastases were negative for both Ki67- and cleaved-caspase-3-staining, regardless of the knockdown of Rif or mDia2 expression. Values = means ± SD (n = 3). (*) $p < 0.05$, (ns) $p > 0.5$.

(B) Effect of Rif-, mDia2- and Cdc42-knockdown on lung colonization by the TS/A cells. The control (sh scrambled), Rif-knockdown, mDia2-knockdown and Cdc42-knockdown TS/A cells, also expressing GFP, were injected into mice via the tail vein. Metastasis formation in the lungs by these cells was analyzed. Shown are the representative images of the left upper lobe of the lungs (left). The number of macroscopic metastases in the left upper lobe of the lungs was also plotted. The red vertical bar represents the mean value in each sample group. (*) $p < 0.005$.

Bars = 100 μm (A [low mag.]), 10 μm (A [high mag.]), 2 mm (B).

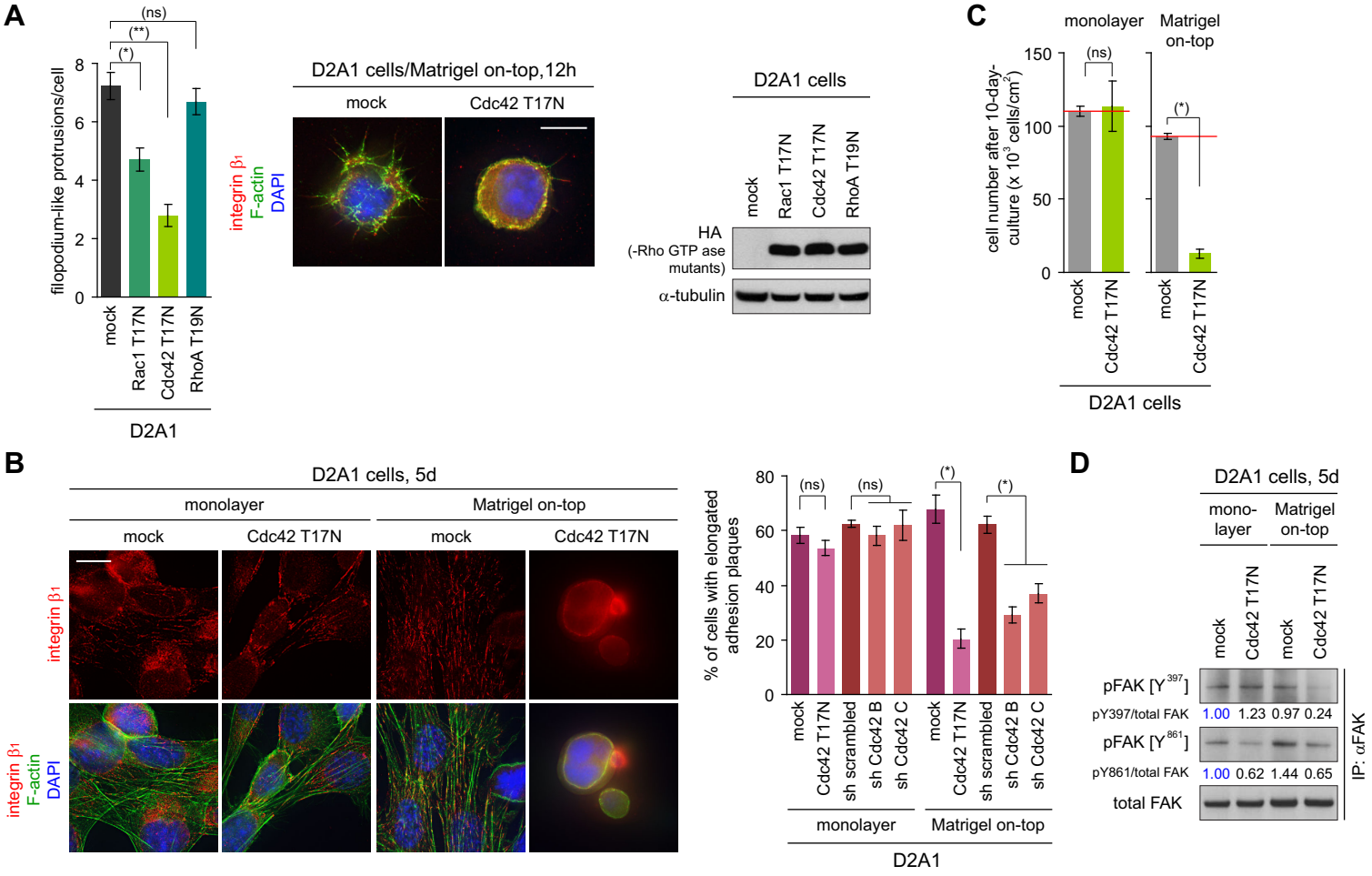

Supplementary Figure S14. Blocking FLP formation and proliferation *in vitro* by the inhibition of Cdc42

(A) Effect of the functional inhibition of Rho GTPases on the formation of FLPs. D2A1 cells expressing one of the dominant-negative mutants of Rac1, Cdc42 and RhoA (Rac1 T17N, Cdc42 T17N and RhoA T19N, respectively; ref. 31) or a control vector (mock) were propagated under MoT conditions for 12 hours and stained for integrin β_1 (red), F-actin (green) and nuclei (by DAPI; blue). The number of FLPs per cell within each cell population was plotted (left). Cdc42 T17N expression diminished FLP formation in these cells more efficiently than did the expression of Rac1 T17N or RhoA T19N. Representative images of mock- and Cdc42 T17N-expressing-D2A1 cells were also presented (middle). The expression levels of these mutants (all had hemagglutinin [HA]-tag at their N-termini) were analyzed by immunoblotting (right); this revealed that these mutants were expressed at comparable levels. (*) $p < 0.002$, (**) $p < 1 \times 10^{-7}$, (ns) $p > 0.5$.

(B) Role of Cdc42 in the formation of integrin β_1-containing, elongated adhesion plaques *in vitro*. Control and Cdc42 T17N-expressing D2A1 cells, as well as Cdc42 knockdown cells (sh Cdc42 B and C) and their control (sh scrambled), were cultured either as a monolayer or under MoT conditions for 5 days and stained for integrin β_1 (red), F-actin (green) and nuclei (by DAPI; blue) (left). The presence of integrin β_1-containing, elongated adhesion plaques within each cell population was quantified (right). (ns) $p > 0.1$, (*) $p < 0.001$.

(C) Role of Cdc42 in cell proliferation *in vitro*. Control and Cdc42 T17N-expressing D2A1 cells were cultured either as a monolayer or under MoT conditions for 10 days and the resulting number of cells was plotted. (ns) $p > 0.7$, (*) $p < 1 \times 10^{-4}$.

(D) Role of Cdc42 in FAK phosphorylation *in vitro*. Control and Cdc42 T17N-expressing D2A1 cells were cultured either as a monolayer or under MoT conditions for 5 days. Cell lysates were immunoprecipitated with an anti-total FAK antibody and the precipitates were analyzed by immunoblotting. Values represent the ratio of band intensities (pFAK/total FAK) relative to that of the sample from the D2A1-mock cells (monolayer).

Bars = 10 μm. Values = means ± SEM (n = 100; A) or means ± SD (n = 3; B,C).

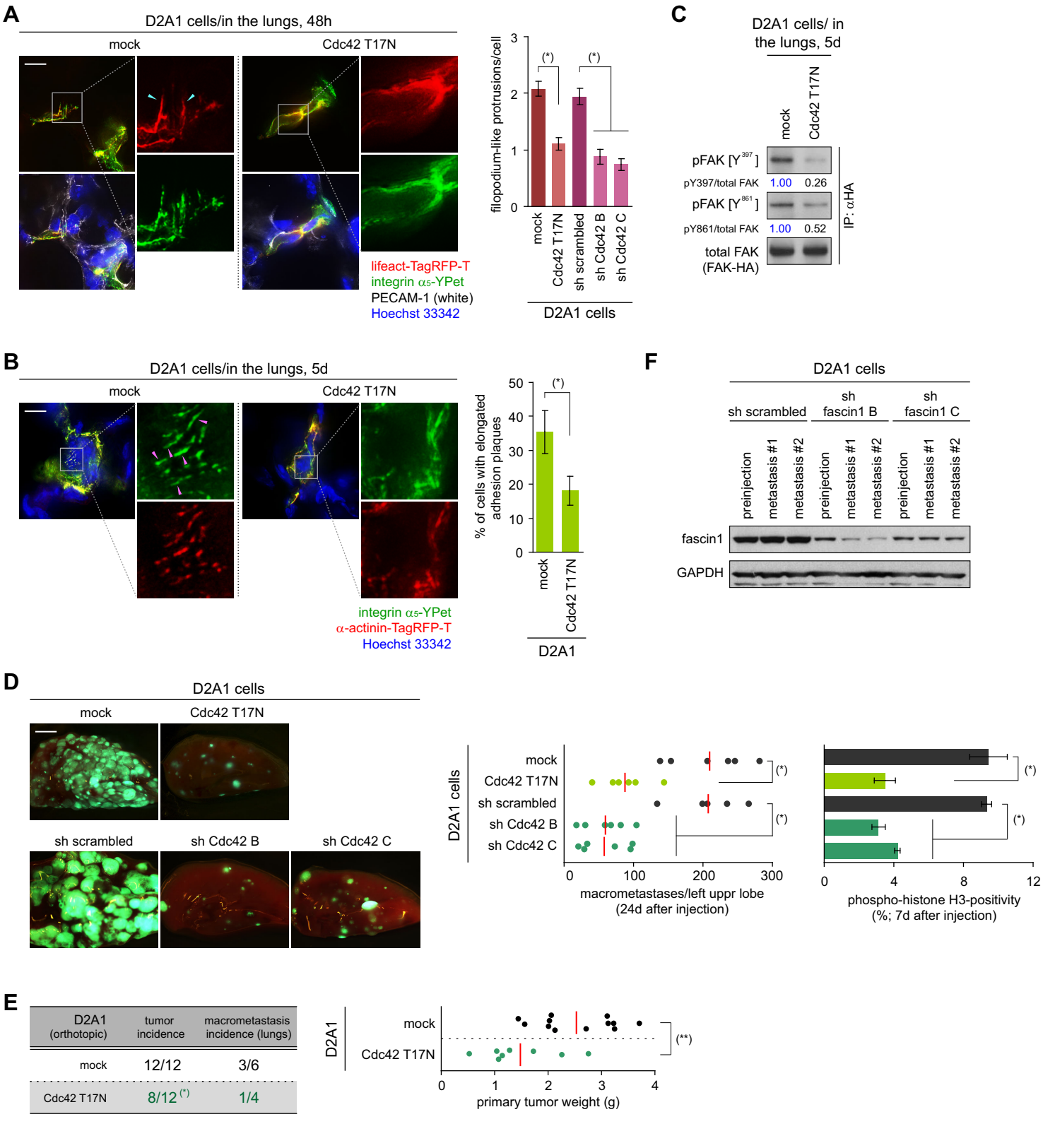

Supplementary Figure S15. Blocking FLP formation and proliferation *in vivo* by the inhibition of Cdc42

(A) Role of Cdc42 in the formation of FLPs *in vivo*. D2A1 cells expressing integrin α_5-YPet (green) and lifeact-Tag-RFP-T (red) were further engineered either to express Cdc42 T17N or to knockdown Cdc42 expression. These and the control cells were tail-vein injected into mice and 2 days later, lungs were harvested and frozen-sectioned. These fluorescent proteins, as well as the blood vessels (by PECAM-1-staining; white) and nuclei (by Hoechst 33342; blue) were visualized on these sections (left). FLPs are indicated by the blue arrowheads. The number of FLPs per cell within each cell population was also plotted (right). (*) $p < 2 \times 10^{-5}$.

(B) Role of Cdc42 in the formation of elongated adhesion plaques *in vivo*. D2A1 cells expressing integrin α_5-YPet (green) and α-actinin-Tag-RFP-T (red) were engineered to express Cdc42 T17N. These and the control cells were tail-vein injected into mice and 5 days later, lungs were harvested and frozen-sectioned. These fluorescent proteins, as well as the nuclei (by Hoechst 33342; blue) were visualized

on these sections (left). The elongated form of adhesion plaques are indicated by the pink arrowheads. The presence of these plaques within each cell population was also quantified (right). (*) $p < 0.03$.

(C) Role of Cdc42 in FAK phosphorylation *in vivo*. The control and Cdc42 T17N-expressing D2A1 cells, both of which also express HA-tagged FAK (FAK-HA), were injected into mice through the tail vein. After mincing and lysing the lung tissue, FAK-HA was immunoprecipitated from the lysate and analyzed by immunoblotting. Values represent the ratio of band intensities (pFAK/total FAK) relative to that of the sample from the D2A1-mock cells.

(D) Role of Cdc42 in metastasis formation following intravenous injection. The metastatic behavior, including the macroscopic colony formation (left, middle) and proliferation (right) in the lung tissue, of the mock- and Cdc42 T17N-expressing D2A1-GFP cells were analyzed. (*) $p < 0.005$.

(E) Inhibition of Cdc42 function and orthotopic tumor formation. The control and Cdc42 T17N-expressing D2A1 cells were injected into mouse mammary fat pads and the subsequent formation of orthotopic tumors as well as the incidence of spontaneous lung metastases were analyzed (bottom). The weight of the primary tumors was also plotted (top). (*) $p < 0.05$ (vs mock) by Fisher's exact test, (**) $p < 0.01$ by Student's *t*-test.

(F) Efficiency of fascin1 knockdown in cells forming the macrometastases. In the experiment whose results are shown in Fig. 6D, the efficiency of fascin1 knockdown in cells obtained from lung metastases (metastasis) as well as in cells before injection (preinjection) was analyzed by immunoblotting. This indicated that the knockdown of fascin1 is retained in the cells forming macrometastases and substantiated our notion that the silencing of fascin1 expression is not disadvantageous for the progression of post-extravasation process of metastasis.

In D (middle) and E (right), the red vertical bar indicates the mean value within each sample group. Bars = 10 μm (A,B), 2 mm (D). Values = means ± SEM ($n = 100$; A) or means ± SD ($n = 3$; B, D [right]).

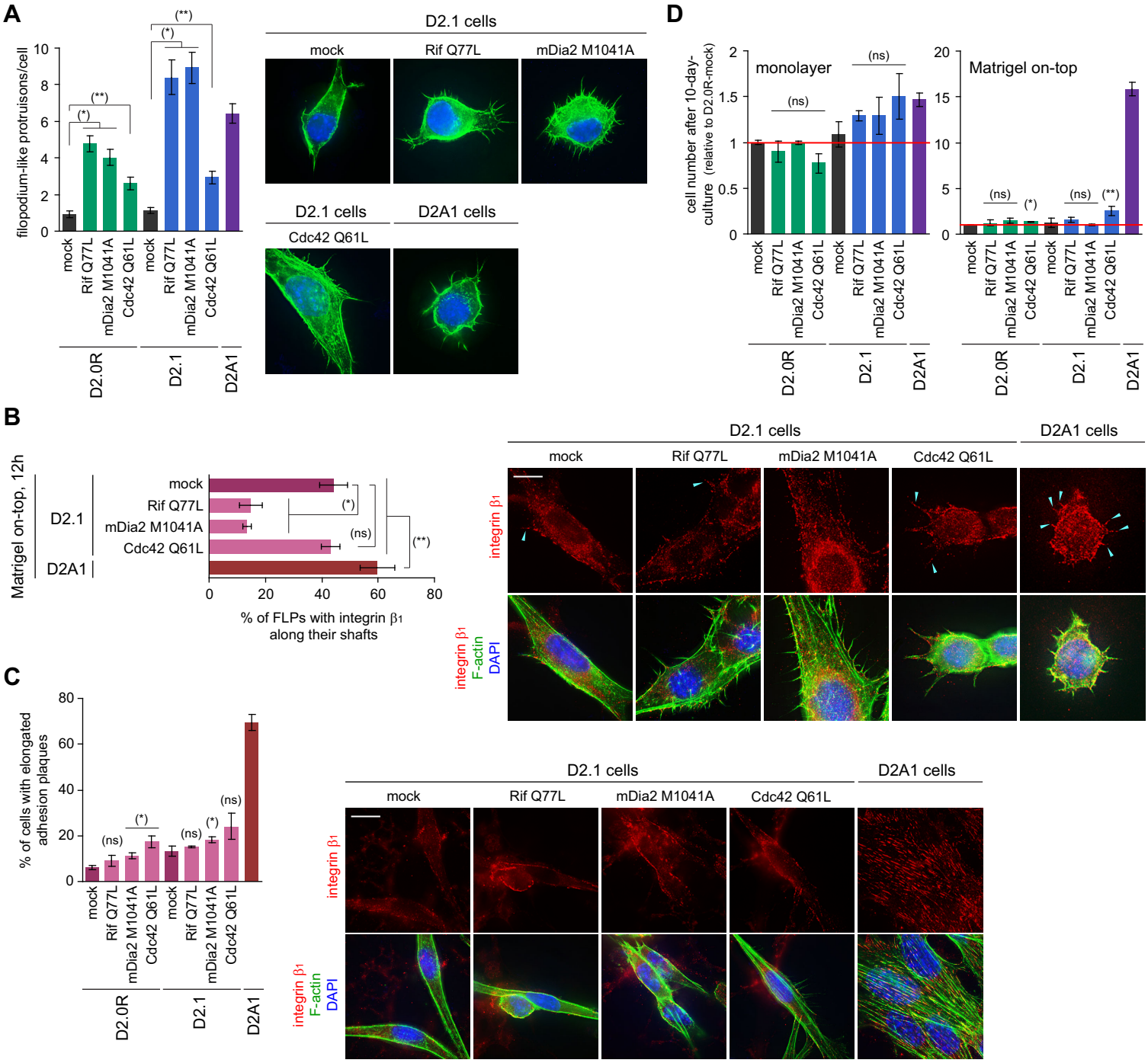

Supplementary Figure S16. Forced induction of FLP formation in the nonaggressive D2.0R and D2.1 cells

(A) FLP formation by the D2.0R and D2.1 cells expressing the constitutively active mutant of Rif, mDia2 or Cdc42. The nonaggressive D2.0R and D2.1 cells were engineered to express the constitutively active mutant of Rif, mDia2 or Cdc42 (Rif Q77L, mDia2 M1041A and Cdc42 Q61L, respectively). These and the control cells (mock), as well as the naturally aggressive D2A1 cells were propagated under the MoT conditions for 12 hours and stained for F-actin (green) and nuclei (by DAPI; blue) (right). The number of FLPs per cell within each cell population was plotted (left). (*) $p < 1 \times 10^{-8}$, (**) $p < 1 \times 10^{-4}$. All the three mutants tested here significantly increased the number of FLPs extended from the D2.0R and D2.1 cells. Notably, the D2.1 cells expressing Rif Q77L or mDia2 M1041A displayed even more abundant FLPs than did the aggressive D2A1 cells.

(B) Localization of integrin β_1 to FLPs that are artificially induced in the D2.1 cells. The engineered D2.1 cells described in A, as well as the D2A1 cells, were propagated under MoT conditions for 12 hours and stained for integrin β_1 (red), F-actin (green) and nuclei (by DAPI; blue). FLPs harboring integrin β_1 along the length of their shafts are indicated by the blue

arrowheads (right). The probability with which the length of the shafts of FLPs was covered by the integrin β_1-staining was plotted for each cell population (left). (ns) $p > 0.7$, (*) $p < 0.005$, (**) $p < 0.03$. FLPs induced by the expression of Rif Q77L and mDia2 M1041A in the D2.1 cells exhibited far lower positivity of integrin β_1-staining than those formed in the aggressive D2A1 cells.

(C) Formation of integrin β_1-containing, elongated forms of adhesion plaques by the D2.0R and D2.1 cells expressing the constitutively active mutant of Rif, mDia2 or Cdc42. The engineered D2.0R and D2.1 cells described in A, as well as the D2A1 cells, were propagated under MoT conditions for 5 days and stained for integrin β_1 (red), F-actin (green) and nuclei (by DAPI; blue) (right). The presence of integrin β_1-containing, elongated adhesion plaques within each cell population was quantified (left). (ns) $p > 0.05$, (*) $p < 0.05$ (vs respective control). While the expression of Rif Q77L, mDia2 M1041A or Cdc42 Q61L – the constitutively active mutants of FLP regulators – enabled the abundant display of FLPs in the D2.0R and D2.1 cells, it only modestly (1.1 to 2.8 fold) increased the percentage of cells that successfully formed integrin β_1-containing, elongated adhesion plaques. The inefficiency of Rif Q77L and mDia2 M1041A, mutants that permitted the D2.1 cells to display even more abundant FLPs than the naturally aggressive D2A1 cells (see A), to restore the formation of adhesion plaques was likely to be due, in part, to the absence of efficient integrin β_1 accumulation in the FLPs induced by the expression of these mutants (see B).

(D) *In vitro* proliferation of the D2.0R and D2.1 cells that express the constitutively active mutant of Rif, mDia2 or Cdc42. The engineered D2.0R and D2.1 cells described in A, as well as the D2A1 cells, were propagated either as a monolayer or under MoT conditions for 10 days. The resulting cell number, relative to that of the D2.0R-mock cells, was plotted. (ns) $p > 0.07$, (*) $p = 0.0004$, (**) $p = 0.03$ (vs respective control).

(E) Effect of Rif Q77L, mDia2 M1041A and Cdc42 Q61L expression on FAK activation under MoT culture conditions. The engineered D2.1 cells described in A, as well as the D2A1 cells, were propagated under MoT conditions for 5 days. Lysates prepared from these cells were subject to immunoprecipitation with an anti-total FAK antibody and the precipitates were analyzed by immunoblotting. Values represent the ratio of band intensities (pFAK/total FAK) relative to that of the control cells. The D2.1 cells manipulated to form abundant FLPs were exhibited far lower levels of FAK phosphorylation than did the naturally aggressive D2A1 cells. This was consistent with the inability of these manipulated D2.1 cells to develop abundant, integrin β_1-containing elongated adhesion plaques (see C), structures that contribute critically to the phosphorylation of FAK (see Fig. 1D). The results shown in C-E collectively indicated that the ability of cells to display abundant FLPs under MoT conditions of culture does not suffice to allow these cells to subsequently develop abundant, mature adhesion plaques in efficient manners, which in turn is critical to the activation of adhesion-dependent, proliferation-promoting signaling events; hence, FLP-forming ability does not necessarily faithfully reflect the proliferation potential of the cells growing under MoT culture conditions.

Bars = 10 μm. Values = means ± SEM ($n = 100$; A) or means ± SD ($n = 3$; B-D).

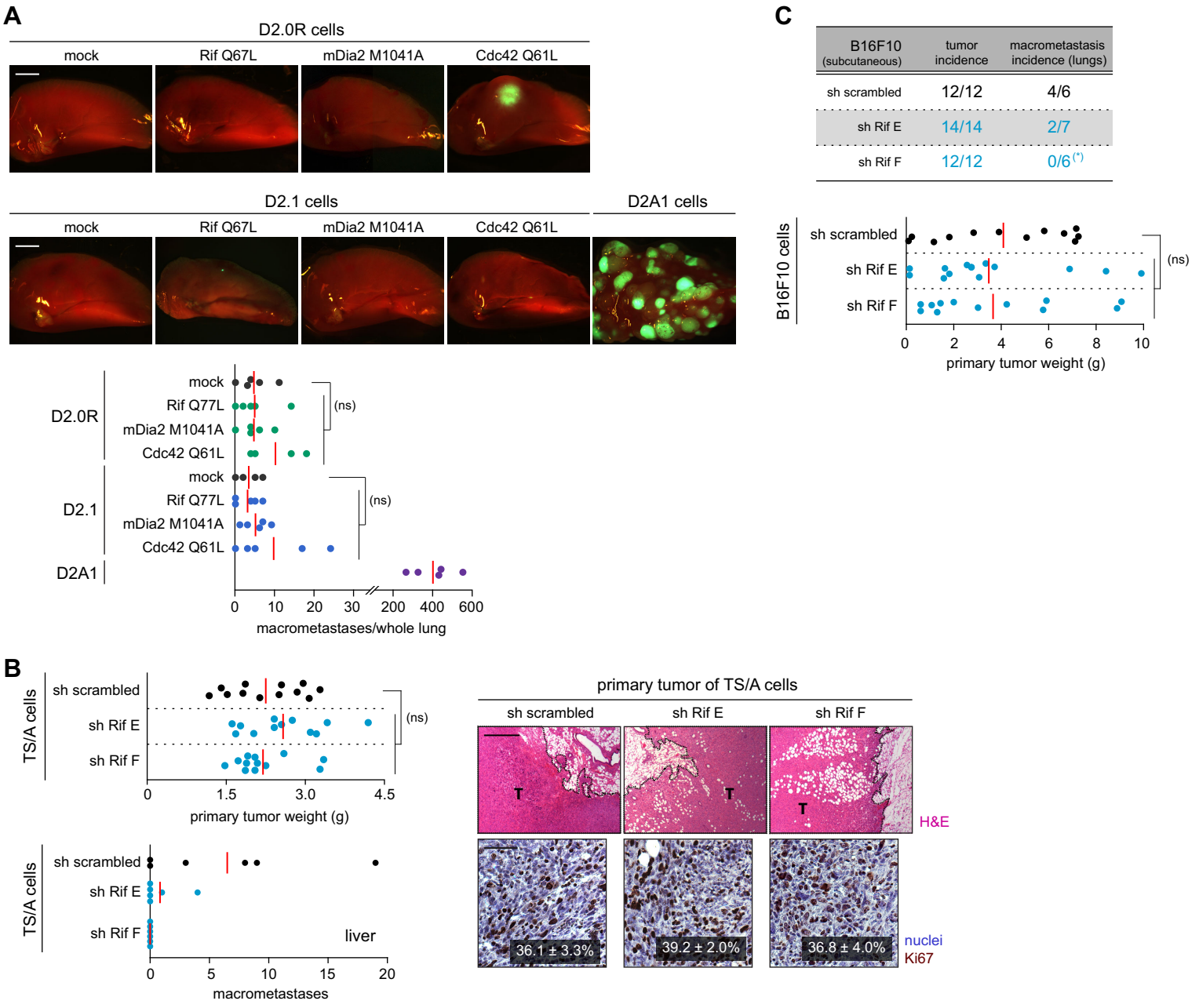

Supplementary Figure S17. *In vivo* behaviors of various cell types after manipulations of FLP-forming ability

(A) Metastatic colonization by the D2.0R and D2.1 cells that express the constitutively active mutant of Rif, mDia2 or Cdc42. D2.0R and D2.1 cells were engineered to express the constitutively active mutant of Rif, mDia2 or Cdc42 (Rif Q77L, mDia2 M1041A and Cdc42 Q61L, respectively). These and the control cells (mock), as well as the naturally aggressive D2A1 cells, all of which also expressed GFP, were injected into mice through the tail vein. Lungs were harvested 42 days (24 days for the D2A1 cells) later. Shown are the representative images of the left upper lobe of the lungs harboring each cell type (top). The number of macroscopic metastases on the surface of the left upper lobe of the lungs was also plotted (bottom). (ns) $p > 0.2$. The red vertical bar represents mean value within each sample group. The manipulations to induce abundant FLP formation in the D2.0R and D2.1 cells did not significantly increase the ability of these cells to develop macroscopic metastases in the lungs. Hence, the potential of the cancer cells to display abundant FLPs appeared to be necessary, but not sufficient, for the ability of these cells to colonize the lung tissue.

(B) Effect of the Rif knockdown on orthotopic tumor formation and liver metastasis by the TS/A cells. In the experiment whose results are shown in Fig. 7C, primary tumors were harvested and weighed (top-left). Subsequently, the paraffin embedded sections of these tumors were prepared, which were subjected to H&E-staining (top-right) and the staining for the proliferation marker Ki67 (bottom-right). The positivity of nuclear Ki67 staining was scored on these sections. Values = means ± SD (n = 3). The number of macroscopic metastases observed on the surface of the liver was also plotted (bottom-left). (ns) $p > 0.2$. See also Fig. 7C.

(C) Role of Rif in subcutaneous tumor formation and spontaneous metastasis of B16F10 cells. The control and Rif-knockdown-B16F10 cells were subcutaneously implanted into mice and subsequent tumor formation as well as the incidence of spontaneous, macroscopic lung metastases were analyzed (top). The weight of the primary tumor was also plotted (bottom). (*) $p < 0.04$ (vs sh scrambled) by Fisher's exact test, (ns) $p > 0.5$ by Student's t-test.

The red vertical bar represents the mean value within each sample group. Bars = 2 mm (A), 1 mm (B; H&E), 0.1 mm (B; Ki67).